A Continental Shelf Pump for CO_2 on the Adélie Land Coast, East Antarctica

Mar C. Arroyo[1] [iD], **Elizabeth H. Shadwick[1,2,3,4]** [iD], **Bronte Tilbrook[2,3,4]** [iD], **Stephen R. Rintoul[2,3,4]** [iD], **and Kazuya Kusahara[5]** [iD]

[1]Virginia Institute of Marine Science, College of William & Mary, Gloucester Point, VA, USA, [2]CSIRO Oceans and Atmosphere, Hobart, Tasmania, Australia, [3]Australian Antarctic Program Partnership, Institute for Marine and Antarctic Studies, University of Tasmania, Hobart, Tasmania, Australia, [4]Centre for Southern Hemisphere Oceans Research, Hobart, Tasmania, Australia, [5]Japan Agency for Marine-Earth Science and Technology, Yokohama, Japan

Abstract We quantify the transport of inorganic carbon from the continental shelf to the deep ocean in Dense Shelf Water (DSW) from the Mertz and Ninnis Polynyas along the Adélie Land coast in East Antarctica. For this purpose, observations of total dissolved inorganic carbon (TCO_2) from two summer hydrographic surveys in 2015 and 2017 were paired with DSW volume transport estimates derived from a coupled ocean-sea ice-ice shelf model to examine the fate of inorganic carbon in DSW from Adélie Land. Transports indicate a net outflow of 227 ± 115 Tg C yr^{-1} with DSW in the postglacial calving configuration of the Mertz Polynya. The greatest outflow of inorganic carbon from the shelf region was delivered through the northern boundary across the Adélie and Mertz Sills, with an additional transport westward from the Mertz Polynya. Inorganic carbon in DSW is derived primarily from inflowing TCO_2-rich modified Circumpolar Deep Water; local processes (biological productivity, air-sea exchange of CO_2, and the addition of brine during sea ice formation) make much smaller contributions. This study proposes that DSW export serves as a continental shelf pump for CO_2 and is a pathway to sequester inorganic carbon from the shallow Antarctic continental shelf to the abyssal ocean, removing CO_2 from atmospheric exchange on the time scale of centuries.

Plain Language Summary Dense waters formed on the Antarctic continental shelf flow into bottom waters that spread throughout the global ocean. These Dense Shelf Waters play an important role in transporting material from the middle and upper layers of the water column to the abyssal ocean. By combining observations and model simulations, we track the transport of dissolved CO_2 in these Dense Shelf Waters from the continental shelf to the deep ocean from the Mertz and Ninnis Polynyas in East Antarctica. We find the largest contributor of dissolved CO_2 to Dense Shelf Water formed in this region is the CO_2-rich midlayers that move onto the continental shelf from offshore. Once on the shelf, local processes in the upper water column further enrich these waters with dissolved CO_2 before their subsequent descent into bottom waters and the abyssal ocean. Our findings highlight the importance of the CO_2-rich midlayers, rather than upper ocean shelf processes, in driving the conditions for carbon sequestration in the deep ocean.

1. Introduction

The Southern Ocean is the central feature connecting the world's ocean basins and plays an integral role in regulating global marine biogeochemical cycles (Marinov et al., 2006; Sarmiento et al., 2004; Sigman & Boyle, 2000). Along the Antarctic continental margins, the production of cold, dense Antarctic Bottom Water (AABW) drives the lower limb of the meridional overturning circulation, delivering oxygen, carbon, and heat to the deep layers of the Atlantic, Indian, and Pacific Oceans during its northward transit (Orsi et al., 1999, 2002). AABW is mainly formed in four regions: the Weddell Sea (Carmack & Foster, 1975), the Ross Sea (Jacobs et al., 1970), Cape Darnley (Ohshima et al., 2013), and along the Adélie Land coast in East Antarctica (Gordon & Tchernia, 1972; Rintoul, 1998). Given its long residence time, AABW has the potential to sequester carbon in the abyssal ocean over centennial time scales and longer, highlighting the importance of this water mass to the global carbon cycle and Earth's climate system (McNeil et al., 2001; Shadwick et al., 2014; Takahashi & Chipman, 2012).
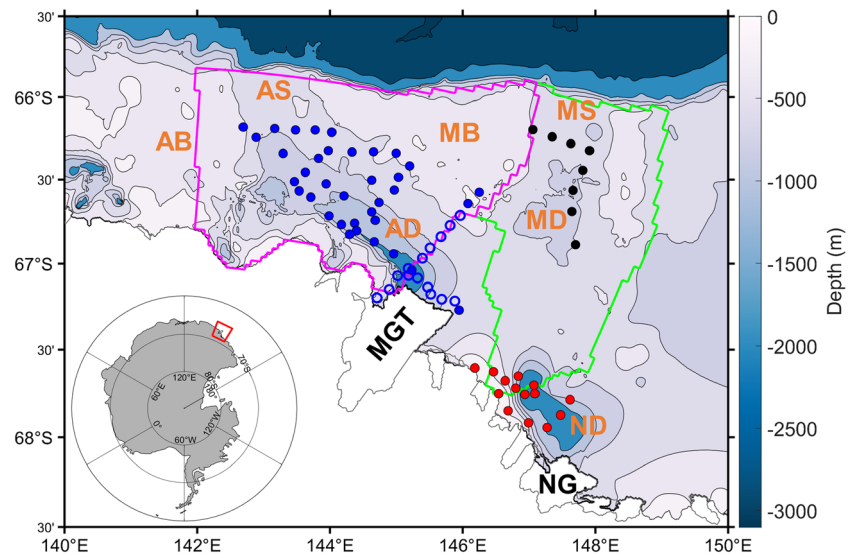
Figure 1. CTD stations in the Mertz Polynya (blue), Ninnis Polynya (red), and Mertz Depression (black) from two summer voyages in January 2015 (AU1402) and January 2017 (AU1602) with bathymetry from the 2019 General Bathymetric Chart of the Oceans (GEBCO Bathymetric Compilation Group, 2019). Repeat stations adjacent to the Mertz Glacier Tongue on the two voyages are indicated with open blue circles. Magenta and green lines delineate model boundaries for the Mertz Polynya and Ninnis Polynya, respectively, from Kusahara et al. (2017). Geomorphic features: Adélie Bank (AB), Adélie Depression (AD), Adélie Sill (AS), Mertz Bank (MB), Mertz Depression (MD), Mertz Glacier Tongue (MGT), Mertz Sill (MS), Ninnis Depression (ND), and Ninnis Glacier (NG).

Coastal polynyas are persistent areas of open water surrounded by sea ice that form in the lee of a coastline or otherwise fixed boundary, such as a glacial tongue or grounded iceberg (Massom et al., 1998; Morales Maqueda et al., 2004). Polynyas are considered to be sinks for atmospheric CO_2 as a result of their high rates of seasonal primary production and associated strong surface CO_2 undersaturation in the spring, when the return of solar radiation to the shallow nutrient-rich surface mixed layer offers the phytoplankton community a relief from light limitation (e.g., Arrigo et al., 2008; Arrigo & van Dijken, 2003; Yager et al., 1995). These regions are also recognized for their enhanced rates of sea ice formation and ocean-ice shelf interactions on the continental shelf (Silvano et al., 2016) leading to the formation of Dense Shelf Water (DSW), the precursor to AABW (Williams et al., 2008, 2010). Sources of AABW in the Australian-Antarctic Basin include overflows of DSW formed in the Mertz and Ninnis Polynya systems of the Adélie Land coast in East Antarctica (Figure 1; Rintoul, 1998; Williams & Bindoff, 2003; Williams et al., 2008, 2010).

Coastal polynyas that are sites of DSW formation are unique environments that serve as a direct pathway for the exchange of CO_2 between the atmosphere and the surface and deep layers of the ocean. This is due to the deep mixing on the continental shelf and the movement of relatively shallow shelf waters to the abyssal layers of the open ocean. The export of carbon from these high-latitude coastal polynya systems may be enhanced by a continental shelf pump (CSP) for CO_2 (e.g., Tsunogai et al., 1999), facilitating the transport of carbon from the surface and midlayers to depth for sequestration and storage on long time scales. The CSP describes the interaction of the solubility and biological pumps of carbon with physical mechanisms that move water from the shallow coastal sea to an adjacent deep ocean. The CSP has been shown to operate in the Northern Hemisphere and sea ice-free systems such as the East China Sea (Tsunogai et al., 1999) and North Sea (Bozec et al., 2005; Thomas et al., 2004) and in the Chukchi Sea in the western Arctic Ocean (Bates, 2006) but has been little explored in the Antarctic coastal regions (Murakami et al., 2020; Takahashi & Chipman, 2012).

This study investigates the potential for a CSP for CO_2 from the Mertz Polynya and Ninnis Polynya in East Antarctica. Using biogeochemical observations from two austral summer surveys, the concentrations of total dissolved inorganic carbon (TCO_2) in DSW are characterized and are paired with model-derived volumetric DSW transport estimates to determine the lateral export of inorganic carbon from Adélie Land coastal waters. The local contributions of inorganic carbon to DSW are determined by net community production

(NCP), estimated from surface deficits in TCO_2, and by air-sea exchange of CO_2, using underway measurements of CO_2 fugacity. The implications of an active CSP in the coastal zone of East Antarctic for Southern Ocean carbon export are discussed.

2. Oceanographic Setting

The Mertz Polynya and Ninnis Polynya are recurring coastal polynyas that form in the Adélie Coast region (142–149°E) in East Antarctica, in the lee of the Mertz Glacier Tongue (MGT) and Ninnis Glacier, respectively (Figure 1). Geomorphic features on the continental shelf in the Adélie Land region include several large bathymetric depressions that connect to the deep ocean through shallow sills. Both polynyas are regions of active DSW formation as a result of their high volumes of winter sea ice production and subsequent release of brine to the surface ocean. Offshore katabatic and synoptic scale winds force sea ice away from the coast and their neighboring glacial tongues, sustaining open water in these polynyas and enhancing the intense sea ice growth (Massom et al., 1998). Brine rejection associated with sea ice production and surface cooling during the austral fall and winter increases the density of surface waters, driving convection and formation of DSW. This rejection of salts to the underlying water column enhances the concentration of dissolved constituents, including total alkalinity (TA) and TCO_2, in parallel with salinity in DSW. Although shipboard oceanographic observations on the Adélie Land coast during winter are limited to one study in the Mertz Polynya (Bindoff et al., 2001; Williams & Bindoff, 2003), the seasonal cycle of water mass transformations recorded by a series of moorings revealed that the Adélie Depression (142–146°E) is the primary source of DSW from the Adélie Land coast (Williams et al., 2008). These observational studies have reported a clockwise circulation in the Adélie Depression in winter. As DSW flows along the southeastern side of the Adélie Depression and exits the continental shelf through the shallow Adélie Sill (142.5–143°E), on-shelf intrusions of relatively warm and salty modified Circumpolar Deep Water (mCDW) enter over the Adélie Sill and flow along the northern side of the Adélie Depression to compensate for the DSW outflow. The majority of DSW that forms is exported in the late winter and early spring when the water mass reaches a critical density to transit northward over the Adélie Sill (Williams et al., 2008, 2010). As DSW cascades down the continental slope, it entrains mCDW to acquire its AABW properties (Williams et al., 2008, 2010).

Williams et al. (2008) estimated an annual mean export of 0.1–0.5 Sv of DSW through the Adélie Sill for water masses with a potential density greater than 27.88 kg m^{-3}. Later work identified a secondary source of DSW from Adélie Land exported across the Mertz Sill (147–148°E) from the Mertz Depression, east of the MGT and north of the Ninnis Polynya (Williams et al., 2010). DSW exported from the Mertz Sill is lighter and fresher than DSW exported from the Adélie Sill, owing to a lower rate of sea ice production over the Mertz Depression compared to over the Adélie Depression (Williams et al., 2010). Several numerical modeling studies agree well with observations in documenting the clockwise gyre circulation and dense water formation in the Adélie Depression (Cougnon et al., 2013; Marsland et al., 2004, 2007) and dense water formation in the Mertz Depression (Kusahara et al., 2010, 2011a).

In the early summer months (November and December), a reduction or cessation of sea ice production and the onset of seasonal sea ice melt freshens and stratifies the water column, reducing or halting DSW formation. The restratification of the water column in summer allows for a more detectable signal of mCDW in the midlayers of the water column due to a pause in convection that erodes warm mCDW in winter (Williams et al., 2008; Williams & Bindoff, 2003). In summer, mCDW is found between the lighter Antarctic Surface Water layer and the denser DSW layer (Williams et al., 2008). In addition to the Adélie Sill, intrusions of mCDW occur across the shelf break near the Mertz Bank and Ninnis Bank as illustrated by model simulations over an annual mean field (Cougnon et al., 2017; Kusahara et al., 2017). The delivery of mCDW into the intermediate layer increases salinity on the continental shelf that preconditions the midwater column with saline water before the onset of sea ice formation and DSW production in the following winter. Because the mCDW water mass primarily derives its biogeochemical properties from the Antarctic Circumpolar Current (ACC; Whitworth et al., 1998), the mCDW inflows are also highly enriched in inorganic nutrients and TCO_2, resulting from the cumulative remineralization of organic matter during its modification over the Antarctic slope and shelf. Wintertime sea ice formation subsequently delivers additional brine to the surface water in the polynyas, further increasing its salinity and density, while concentrating dissolved salts, including TCO_2.

This cold, saline DSW is then bathymetrically steered in the shelf depressions as outflows across the Adélie and Mertz Sills at the continental shelf break.

The Mertz Polynya was the third largest producer of sea ice among all Antarctic polynyas until early 2010 when the terminal end of the MGT separated from the Mertz Glacier after impact with the iceberg B9b. The MGT calving event dramatically reduced polynya size and total sea ice production (Shadwick et al., 2013; Tamura et al., 2012) and subsequently the density and volume of DSW on the continental shelf (Lacarra et al., 2014). Observations following the MGT calving show evidence for continued formation of DSW (Snow et al., 2018) and changes to local biogeochemical cycling (Shadwick et al., 2017).

Some of the DSW formed during the winter season accumulates in the deep Adélie, Mertz, and Ninnis Depressions (Lacarra et al., 2014; Williams et al., 2008, 2010). These depressions thereby act as reservoirs, where DSW can be observed in the subsequent summer (e.g., Lacarra et al., 2014; Shadwick et al., 2013). Accumulated DSW signatures are isolated from lateral exchange off the shelf break by the shallow sill barriers and by the presence of less dense mCDW in the intermediate water column. Accordingly, the bottom waters observed within the on-shelf depressions of the Mertz and Ninnis Polynyas during the summer surveys presented in this study are taken to be indicative of the DSW produced during the previous winter season.

3. Methods

This study uses hydrographic and CO_2-system data collected on the continental shelf of the Adélie Land coast (142–149°E) during two summer cruises in January 2015 (AU1402) and 2017 (AU1602) on board the RSV *Aurora Australis* following the MGT calving in 2010 (Figure 1). The AU1402 voyage includes 51 conductivity-temperature-depth (CTD) stations occupied between 9 and 17 January 2015 in the Adélie Depression and along the western edge of the MGT (Rosenberg, 2020). An additional 37 CTD stations were made on the AU1602 voyage between 14 and 21 January 2017 and extended farther east on the Adélie Land coast (Rosenberg & Rintoul, 2018). The AU1602 data set encompasses 15 CTD stations adjacent to the MGT that were repeated from AU1402 (see Figure 1, open circles) as well as 14 CTD stations within the Ninnis Polynya and 8 CTD stations in the Mertz Depression.

On both voyages, CTD deployments obtained continuous measurements of 2-dbar averaged practical salinity, temperature (°C), and pressure (dbar) using a SeaBird SBE9plus CTD (serial 704) with dual temperature and conductivity sensors. The accuracies of temperature and salinity were ~0.001°C and ~0.002, respectively. Similarly, continuous measurements of 2-dbar averaged dissolved oxygen (μmol kg^{-1}) were made with SBE 43 (serial 0178) in agreement to within 1% of discretely sampled dissolved oxygen samples. The CTD was mounted on a rosette frame with 22 × 10 L General Oceanic Niskin bottles on the AU1402 voyage and with up to 24 × 10 L Niskin bottles on AU1602.

3.1. Underway fCO$_2$ Measurements and Air-Sea CO$_2$ Flux Calculations

High-frequency underway measurements of the fugacity of carbon dioxide (fCO$_2$), sea surface salinity, and sea surface temperature (SST) were taken from the seawater intake ~4 m below the ocean surface along the cruise tracks of both voyages. Measurements of fCO$_2$ were made using a nondispersive infrared gas spectrometer (LI-COR, LI-7000) with continuous flow equilibration corrected to in situ underway temperature and salinity and to 100% humidity (Pierrot et al., 2009). Travel time between the seawater intake and the CO_2 system on board was approximately 70 s, resulting in ≤0.6°C warming. Underway fCO$_2$ measurements were calibrated every 3–4 hr with a set of four reference standards (0, 299.41, 353.00, and 402.15 μatm on AU1402; 0, 255.93, 380.52, and 451.12 μatm on AU1602) on the WMO-X2007 mole fraction scale for CO_2 in dry air (Zhao & Tans, 2006). The atmospheric mole fraction of CO_2 was measured every 4 hr at ~16 m above sea level and used to calculate atmospheric fCO$_2$. Uncertainties were ±2 μatm for seawater fCO$_2$ and ±0.2 μatm for atmospheric fCO$_2$.

Air-sea fluxes of CO_2 were calculated using the equation

$$F_{CO_2} = k \ \alpha \ \Delta f CO_2 \qquad (1)$$

where F_{CO_2} is the CO_2 flux (mmol C m^{-2} day^{-1}), k is the gas transfer velocity, and α is the solubility of

CO_2 (Weiss, 1974). $\Delta f CO_2$ (µatm) is the gradient of $f CO_2$ between the sea surface and the atmosphere ($f CO_2^{sea} - f CO_2^{air}$), where a negative flux indicates an ocean uptake of atmospheric CO_2. The gas transfer term (k; cm hr^{-1}) was parameterized following Wanninkhof (2014) given by

$$k = 0.251 \, U_{10\,m}^2 \, (Sc/660)^{-0.5} \tag{2}$$

using daily averaged winds from 10 m above the sea surface (U_{10}; m^2) obtained from the NCEP/NCAR Reanalysis product (Kalnay et al., 1996) and corrected to a Schmidt (Sc) number of 660. The uncertainty in CO_2 flux was determined by comparing F_{CO_2} values parameterized by several gas transfer velocities (Ho et al., 2006; Sweeney et al., 2007; Wanninkhof, 1992) and was better than 1 mmol C m^{-2} day^{-1}.

3.2. Discrete CO_2 System and Biogeochemical Observations

Discrete measurements of TCO_2 and alkalinity (TA) were made at each station following analytical methods described in Dickson et al. (2007). Upon sampling, a saturated solution of mercuric chloride was added to each sample to halt biological activity. TCO_2 concentrations were either determined on board (AU1402) or stored in the dark at 4°C until analysis at CSIRO in Hobart (AU1602) by coulometric titration using a Single Operator Multiparameter Metabolic Analyzer (SOMMA) system (Johnson et al., 1993). TA concentrations were determined on board both voyages by automatic open-cell potentiometric titration with 0.1 M hydrochloric acid using a Methrom Titrando system. All analyses were routinely checked with Certified Reference Materials (CRMs Batch #137 on AU1402; #145 and #153 in AU1602) provided by A. G. Dickson at Scripps Institution of Oceanography (Dickson et al., 2003). Verified analytical uncertainties were better than ± 1.4 µmol kg^{-1} for TCO_2 and ± 1.5 µmol kg^{-1} for TA for AU1402 and better than ± 1.5 µmol kg^{-1} for TCO_2 and ± 1 µmol kg^{-1} for TA for AU1602.

3.3. Seasonal Changes in TCO_2 and NCP Computations

The summertime distribution of mixed-layer TCO_2 is influenced by a combination of physical and biological processes. The mixed layer depth (MLD) was defined as the depth at which potential density anomaly exceeds a reference measurement at 10 m by 0.01 kg m^{-3} (e.g., Lacarra et al., 2011; Shadwick et al., 2014). Deficits in TCO_2 (mmol m^{-2}) were computed at each station as the depth-integrated difference between an inferred winter TCO_2 concentration and the observed summer TCO_2 concentrations in the mixed layer, defined by the equation

$$\text{Total mixed-layer } TCO_2 \text{ deficit} = \int_0^{MLD} TCO_2^{winter} - TCO_2^{summer} \, dx \tag{3}$$

Profiles of TCO_2 show that concentrations were nearly constant below 125 m in both sampling years (see Figures 4c and 6d). The inferred winter TCO_2 was therefore defined as the average value at 150 m depth in the combined AU1402 and AU1602 data sets ($TCO_2^{winter} = 2{,}230$ µmol kg^{-1}; standard deviation = 4 µmol kg^{-1}; $n = 33$). This approach in determining winter TCO_2 follows previous studies in East Antarctic polynyas (e.g., Arroyo et al., 2019; Shadwick et al., 2014) as the temperature minimum on the shelf was not clearly defined and influenced by the presence of Ice Shelf Water (ISW).

The total deficit in TCO_2 in the mixed layer (Equation 3) was partitioned into biological and physical drivers, following the methods of Shadwick et al. (2017). TCO_2 deficits were attributed to changes due to (1) salinity, determined as the difference between observed TCO_2 and salinity-normalized TCO_2, normalized to an inferred winter salinity of 34.45 (mean salinity at 150 m); (2) calcium carbonate processes, determined as half of the difference between observed TA and salinity-normalized TA, after correcting for the influence of nitrate (e.g., Brewer & Goldman, 1976; Jones et al., 2010). TA increases and decreases twice as much as TCO_2 due to calcium carbonate dissolution and precipitation, respectively; (3) biological processes and air-sea CO_2 exchange were determined by difference and are represented in a single term.

In addition to mixed-layer TCO_2 deficits, the reduction in TCO_2 due to biological processes was computed from the surface to 100 m at each station to account for deeper mixing prior to the sampling event. Biological TCO_2 deficits (mol C m^{-2}) were calculated as the depth-integrated difference between the observed summer salinity-normalized TCO_2 and salinity-normalized TCO_2^{winter} from the surface to

100 m. TCO_2 (and TA) concentrations were normalized to the observed area-averaged salinity ($S = 34.5$) to account for the impact of seasonal sea ice melt and (horizontal and vertical) mixing using the conventional method that assumes a zero freshwater end-member value (e.g., Shadwick et al., 2014, 2017; Sweeney et al., 2000). This technique has been shown to overestimate salinity-normalized TA in the coastal Antarctic (e.g., Legge et al., 2017), but too few observational data are available to accurately constrain the freshwater (meteoric and sea ice) TCO_2 and TA end-members in the East Antarctic.

Rates of NCP, defined as the difference between net primary production and heterotrophic respiration, were computed by dividing the 100 m biological TCO_2 deficits over the observed growing season, from start of the productive season until the time of sampling in January. The start of the productive season was defined as 1 November for each sampling year based on the onset of primary production inferred from monthly averaged chlorophyll *a* concentration derived from the MODIS-Aqua satellite product at 9-km resolution and Level 3 processing (https://oceancolor.gsfc.nasa.gov/l3/). This approach simply assumes a constant daily rate of biological carbon uptake since 1 November (which more accurately varies over the progression of the growing season) and does not account for air-sea CO_2 fluxes. The reported 100 m TCO_2 deficits and NCP values likely reflect a lower bound of the total biological uptake over the entire productive season that continues after the sampling event.

3.4. Inorganic Carbon Transport With DSW

Volumetric DSW transport estimates were derived from a coupled ocean-sea ice-ice shelf model described in Kusahara et al. (2017). This circumpolar Southern Ocean numerical model uses an orthogonal, curvilinear coordinate system with enhanced horizontal resolution (~5–7 km) in the Adélie Land region and a hybrid σ/z vertical coordinate. Bathymetry is derived from the General Bathymetric Chart of the Oceans (GEBCO, IOC et al., 2003), and ice shelf draft is derived from the 1-min refined topography (RTopo-1, Timmermann et al., 2010). Simulations quantify DSW formation in the Mertz and Ninnis Polynyas on the Adélie Land coast, as well as its export from the shelf break on monthly time scales from the Mertz Depression/Sill and the Adélie Depression/Sill that are consistent with previous observational studies on the continental slope and rise (Kusahara et al., 2011a; Williams et al., 2010). Volume transports for the Mertz Polynya and Ninnis polynya represent outflows and inflows of DSW through western, northern, and eastern boundaries of each polynya, as delineated by Kusahara et al. (2017) (Figure 1). This ocean model comprehensively reproduced key proceses in coastal polynyas including sea ice production, basal ice shelf melting, whole-water column structure, and DSW formation and export over different time scales (i.e., seasonal, annual, and interannual) as well as the distribution of AABW over the continental slope and rise (Kusahara et al., 2017). Model simulations were performed under two scenarios: before and after the 2010 MGT calving event. For the analysis in the present study, the monthly DSW transport estimates were averaged in the postcalving simulation (C2000 case) in which the MGT calved on 1 January 2000. Although the actual MGT calving event occurred in February 2010, the analysis by Kusahara et al. (2017) found that there are no pronounced differences in DSW formation and export during model simulations that assume a calving event on 1 January 2000 (C2000) or 1 January 2010 (C2010) during the period of overlap (2010–2013), demonstrating that the numerical results are independent of the timing of the MGT calving. Simulated DSW transport estimates were averaged by month from January 2001 to December 2013 to obtain a long-term field. The dramatic changes to the local icescape and ocean circulation on the Adélie Land coast following the MGT calving has led to an evolving definition of the critical density criterion for DSW outflow from the Adélie and Mertz Depression regions (e.g., Kusahara et al., 2011b). In this study, we use the criteria of $\sigma_\theta \geq 27.88$ kg m^{-3} for DSW exported from the Mertz Polynya and $\sigma_\theta \geq 27.84$ kg m^{-3} from the Ninnis Polynya.

To determine the amount of inorganic carbon that is transported with DSW from the Adélie Land coast, these model-derived volumetric DSW transport estimates, binned by potential density in intervals of 0.02 kg m^{-3}, are combined with TCO_2 concentrations in DSW observed at depth in each summer study. Because the deep depressions act as reservoirs for DSW formed during the previous winter, the summer observations of TCO_2 below $\sigma_\theta \geq 27.84$ kg m^{-3} and $\theta \leq -0.5°C$ are assumed to be representative of the winter concentration in DSW. Profiles of TCO_2 for repeated stations in January 2015 and 2017 adjacent to the MGT show excellent agreement in concentration, particularly in the DSW water mass (depths greater than ~700 m) between the two years, suggesting the interannual variability in subsurface TCO_2 is small

Table 1
Bin-Averaged TCO₂ Concentrations ($\mu mol\ kg^{-1}$) in DSW on the Adélie Land Coast

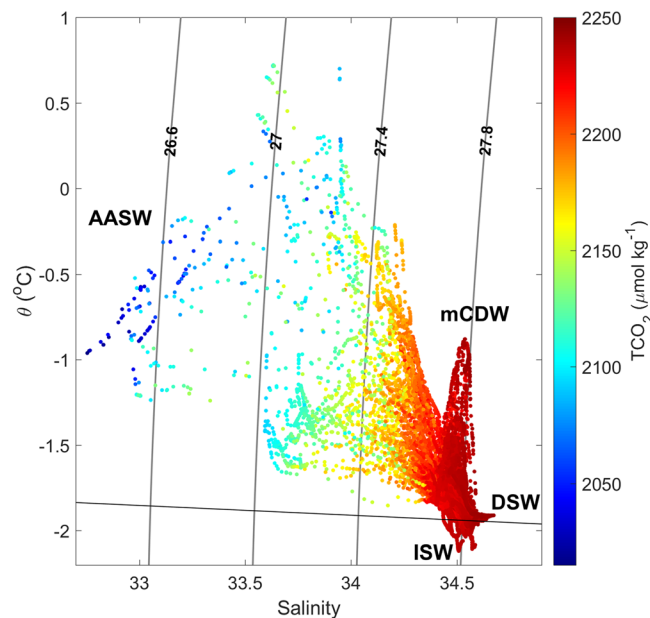| DSW bin (kg m⁻³)	TCO₂ (µmol kg⁻¹)	No. of Obs.
27.85	2,238 ± 2	71
27.87	2,239 ± 2	45
27.89	2,240 ± 2	20
27.91	2,241 ± 2	44
27.93	2,243 ± 1	11

Note. The value of DSW bin concentration (± standard deviations) is the midpoint between two bins and the corresponding number of discrete bottle observations (No. of Obs.) from January 2015 and January 2017. Any volume of DSW denser than observed in the summer is assigned the concentration in the 27.93 kg m⁻³ bin.

(Figure 1, open circles; see also Figure 4). Thus, TCO₂ values in DSW from the 2015 and 2017 data sets are combined and are treated as one. Discrete TCO₂ measurements at each station were linearly interpolated between sampling depths to the 2-dbar vertical resolution of the CTD measurements. Similar to the model outputs, TCO₂ values were binned by potential density intervals in increments of 0.02 kg m⁻³ and were averaged to yield one TCO₂ value per density bin (Table 1). The standard deviations of TCO₂ measurements within each bin are small (1–2 µmol kg⁻¹) and similar to the analytical uncertainty (1.5 µmol kg⁻¹), giving confidence that these signatures are representative of the water in a particular bin. Water masses that were denser than those observed during summer (i.e., $\sigma_\theta > 27.92$ kg m⁻³) were assigned TCO₂ values of the densest observation (i.e., mean TCO₂ between 27.90 kg m⁻³ $< \sigma_\theta <$ 27.92 kg m⁻³).

Inorganic carbon transport in DSW (CO_2^{DSW}; g C s⁻¹) was computed by the following equation

$$CO_2^{DSW} = Transport^{DSW} \times TCO_2^{DSW} \times \rho^{DSW} \times m_c \qquad (4)$$

where $Transport^{DSW}$ is the monthly averaged volume transport (Sv; 10^6 m³ s⁻¹) from the numerical model, TCO_2^{DSW} (µmol kg⁻¹) and ρ^{DSW} (kg m⁻³) are the mean TCO₂ concentration and density, respectively, within each σ^θ bin (Table 1), and m_c is the molar mass of carbon (g C mol⁻¹). The CO_2^{DSW} computations were scaled from units of g C s⁻¹ to g C month⁻¹ and to g C yr⁻¹ by multiplying the estimated CO_2^{DSW} by the number of seconds in each month and in one year, respectively, to yield seasonal and annual CO_2^{DSW} values from both the Mertz and Ninnis Polynyas. Net CO_2^{DSW} is calculated as the difference between outflowing and inflowing CO_2^{DSW} (i.e., positive values indicate export). Here, it is assumed that there is no seasonal variability in TCO_2^{DSW} within each σ^θ bin, and the uncertainties reported are due to model transport interannual variability alone, given by the standard deviation of the scenario years ($n = 13$).

4. Results

4.1. Hydrographic Properties

Water mass characteristics on the Adélie Land coast during the 2015 and 2017 voyages were similar to those observed in previous summer studies (Lacarra et al., 2011; Shadwick et al., 2014, 2017; Figure 2). The surface waters were relatively warm and low saline, characteristic of Antarctic Surface Water (AASW) properties in summer (Figures 2 and 3). Underway measurements taken along the cruise tracks indicate sea surface salinity was greater in the study region in 2015 (~33.7 to 34.5) as compared to 2017 (~32.6 to 33.9), suggesting a larger volume of sea ice melt and a resulting surface freshening prior to the 2017 voyage (Figures 3a and 3b). In both years, relatively low salinity waters were found adjacent to the seaward edge of the MGT. In 2017, salinity reached a maximum within the Ninnis Polynya and decreased latitudinally away from the coast overlying the Mertz Bank and Mertz Depression. Surface waters were often cooler in the Adélie Depression in 2015 (~ −1.6°C to 0.1°C) and west of the MGT as compared to more widely varying SST during the 2017 voyage (~ −1.6°C to 1.0°C) east of the MGT, where increased surface temperatures were likely the result of seasonal warming (Figures 3c and 3d).

Below the summer mixed layer, relatively warm mCDW and cold ISW occupied the intermediate depths above the DSW layer. We define the

Figure 2. Potential temperature (θ, °C)-salinity diagram for CTD measurements from January 2015 and 2017 with contours (gray lines) of potential density anomaly (kg m⁻³) and colors for TCO₂ concentration (µmol kg⁻¹) interpolated to 2 dbar from discrete bottle samples. The black solid line indicates the freezing point of seawater at 50 dbar. Water masses are labeled as Antarctic Surface Water (AASW), modified Circumpolar Deep Water (mCDW), Ice Shelf Water (ISW), and Dense Shelf Water (DSW).

upper limit of mCDW by a potential density of 27.725 kg m^{-3} and ISW by potential temperatures below the surface freezing point at 50 dbar (Aoki et al., 2017). Intrusions of mCDW from offshore of the shelf break deliver a source of high salinity, low dissolved oxygen water to the region. As mCDW is isolated from exchange with the sea surface, it is also enriched in TCO_2 and inorganic nutrients due to the cumulative influence of organic matter remineralization over longer time scales (Figure 2). The signals of ISW near the MGT, formed during the interactions of DSW with the ice shelf, are more evident in summer because the water mass is not yet mixed away by deep winter convection.

CTD stations in January 2015 were repeated in January 2017 in the Mertz Polynya along the MGT (Figure 1, open circles; Figure 4). In both occupations, the bottom waters were relatively cold and salty compared to surface waters. Surface waters in summer 2017 were relatively fresher (~32.8 vs. 33.6) and warmer (~0.5°C vs. −1.0°C) than in summer 2015. The distribution of salinity in both years was nearly uniform with depth below 500 m; however, the subsurface water column salinity was generally greater in 2017 than in 2015, increasing to salinity values of 34.67 and 34.61 near the seafloor, respectively. Profiles of potential temperature are much more variable above 500 m but converge in both years to a bottom temperature of ~1.91°C.

Vertical profiles of TCO_2 and TA concentrations show surface water concentrations of both TCO_2 and TA were lower in January 2017 than in January 2015, due to lower sea surface salinity and increased biological production (discussed below). The impact of the increased subsurface salinity is seen more dramatically in TA (Figure 4d), where subsurface TA concentrations were greater in 2017 than in 2015. An increase in TCO_2 concentration at depth in 2017 relative to 2015 is not seen, and the subsurface concentrations of TCO_2 converged at depth along the MGT. The absence in TCO_2 increase in depth could be attributed to the larger seasonal changes in TCO_2, which is affected by both changes in salinity and biological processes, relative to TA, which is predominantly impacted by changes in salinity (and to a lesser extent biological processes). The increased sensitivity of TA to changes in salinity relative to TCO_2 would mask the apparent trend in subsurface TCO_2. Below 500 m, the average ratio of TCO_2 to TA is consistent between the two sampling years (0.9575 ± 0.0008 in January 2015 and 0.9556 ± 0.0011 in January 2017), and within the analytical uncertainty, suggesting that the increase in subsurface TA (or the absence of subsurface TCO_2 increase) is overall small.

4.2. Surface fCO$_2$ and Air-Sea CO$_2$ Exchange

All surface seawater fCO$_2$ measurements on both voyages were undersaturated with respect to the atmospheric value (382 ± 1.2 µatm in January 2015 and 389 ± 0.6 µatm in January 2017), resulting in a net air-to-sea flux of CO_2 during the observation periods (Figures 3e and 3f). In both years, the distribution of fCO$_2$ exhibited a latitudinal gradient, with a larger degree of undersaturation found adjacent to the coast. Areas of cooler, fresher water in the Adélie Depression correspond to minimum values of fCO$_2$, in contrast to the cooler waters farther offshore in the Mertz Bank associated with maximum values of fCO$_2$. The range of fCO$_2$ values was smaller (~210 to 350 µatm) between the Adélie Depression and the MGT in 2015 compared to fCO$_2$ values on the eastern side (~160 to 382 µatm) of the Adélie Land coast in 2017. In 2017, surface waters adjacent to the MGT and within the Ninnis Polynya exhibited the largest degree of undersaturation, with fCO$_2$ values as low as 150 µatm, consistent with reported elevated dissolved oxygen to argon ratio ($\Delta O_2/Ar$) found in these regions (Moreau et al., 2019).

The Adélie Land coastal region was a moderate sink for atmospheric CO_2 during the austral summers of 2015 and 2017 (Figures 3e and 3f; Table 2). Although the direction of gas exchange was consistently in the direction of oceanic uptake, the magnitude of CO_2 flux varied regionally and between years. Wind speeds were variable in both years, with daily mean wind speeds ranging between 2.1 and 5.8 m s^{-1} in 2015 (mean and standard deviation: 3.9 ± 1.2 m s^{-1}) and between 2.1 and 11.8 m s^{-1} in 2017 (mean and standard deviation: 5.9 ± 3.1 m s^{-1}). Highly undersaturated waters near the MGT recorded the largest ingassing flux in both years (~7 mmol C m^{-2} day^{-1} in 2015 and ~15 mmol C m^{-2} day^{-1} in 2017) consistent with previous studies near the postcalving MGT (Shadwick et al., 2014, 2017). Smaller CO_2 sinks were estimated in the Adélie Depression and near the edge of the continental shelf west of the MGT at 66°S (1 to 5 mmol C m^{-2} day^{-1}). Although surface waters in the Ninnis Polynya were highly undersaturated in fCO$_2$ (−239 < Δ fCO$_2$ < −100 µatm), lower wind speeds resulted in a relatively weaker flux (~2 to
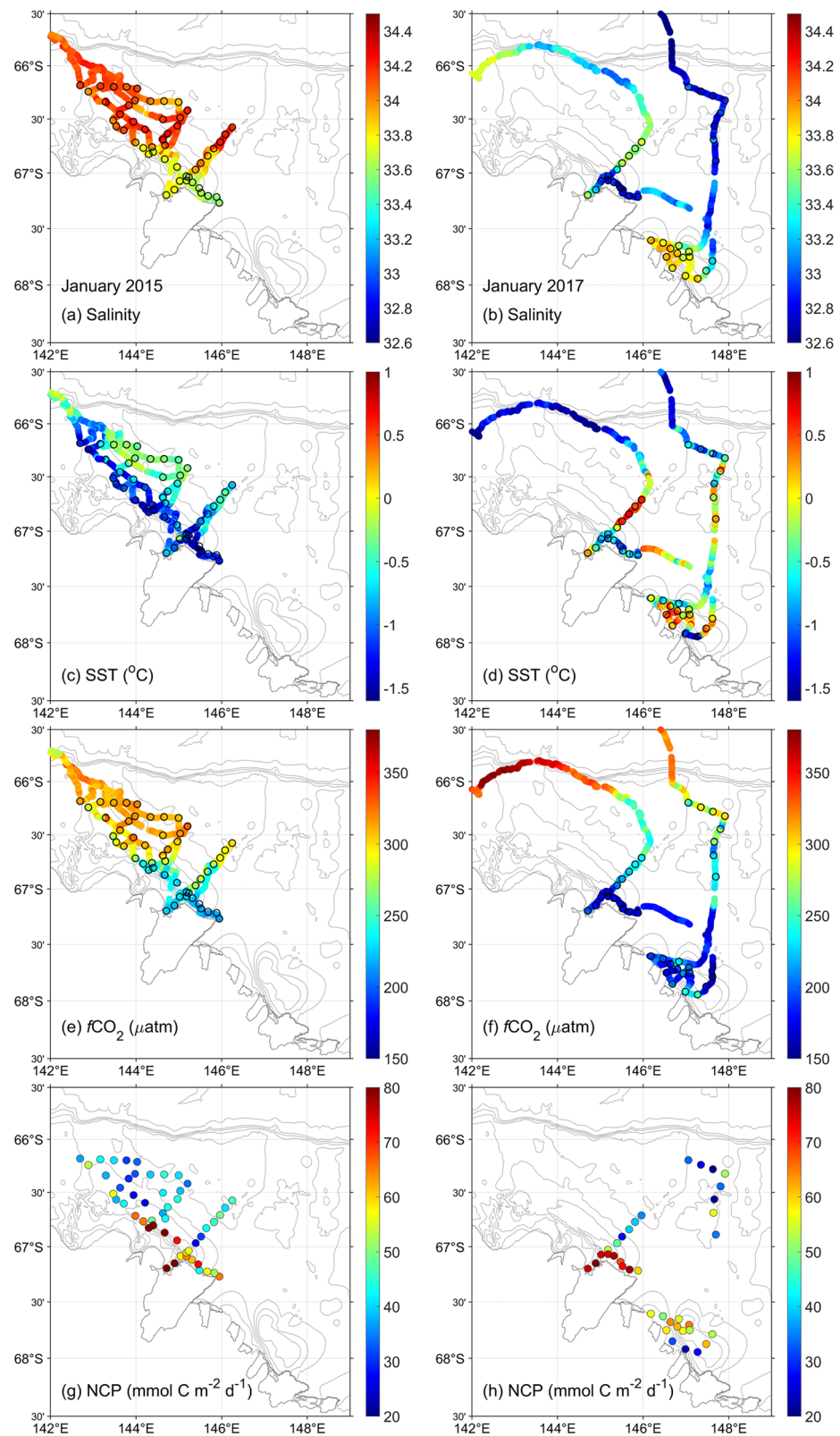
Figure 3. Underway measurements from January 2015 (left column) and January 2017 (right column) for (a, b) salinity, (c, d) sea surface temperature (SST; °C), and (e, f) fCO$_2$ (μatm) and CTD station (g, h) NCP (mmol C m^{-2} day^{-1}) on the Adélie Land coast. Mean observed atmospheric fCO$_2$ values were 382 and 389 μatm in 2015 and 2017, respectively. Open black circles in a–f denote CTD station locations.
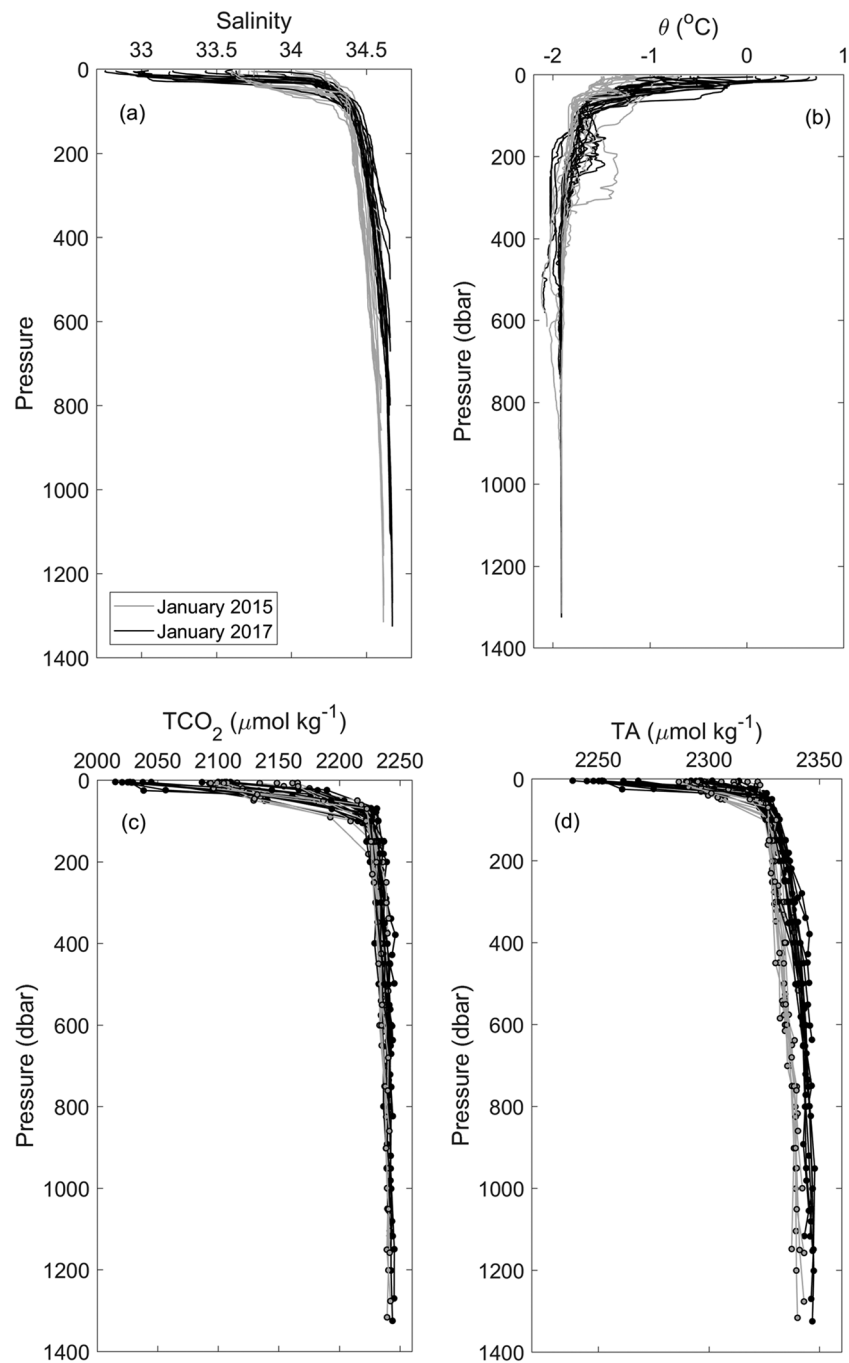
Figure 4. Vertical profiles of (a) CTD salinity, (b) CTD potential temperature (θ; °C), (c) TCO_2 (μmol kg^{-1}), and (d) TA (μmol kg^{-1}) from overlapped stations in the Mertz Polynya adjacent to the MGT from the January 2015 (gray) and January 2017 (black) voyages. See Figure 1 (open blue circles) for CTD station locations.

4 mmol C m^{-2} day^{-1}). The Adélie Land coast was a sink for atmospheric CO_2 with an average flux of approximately 6.6 mmol C m^{-2} day^{-1} over both cruise years.

4.3. CO_2 System Properties

The relationships of TCO_2 and TA with salinity are shown in Figure 5. The concentrations of TCO_2 and TA ranged from 2,015 to 2,245 and from 2,240 to 2,350 μmol kg^{-1}, respectively, over a salinity range of

Table 2

Regional Air-Sea CO_2 Exchange (mmol C m^{-2} day^{-1}), Biological TCO_2 Deficits in the Upper 100 m (mol C m^{-2}), and NCP (mmol C m^{-2} day^{-1}) With Standard Deviations on the Adélie Land Coast

Region	Air-sea CO_2 flux (mmol C m^{-2} day^{-1})	TCO_2 deficit (mol C m^{-2})	NCP (mmol C m^{-2} day^{-1})
Adélie Depression	−3.2 ± 2.6	3.5 ± 1.3	47 ± 18
MGT 2015	−5.0 ± 2.4	4.0 ± 1.1	54 ± 15
MGT 2017	−14.1 ± 7.2	4.3 ± 1.4	62 ± 20
Ninnis Polynya	−4.6 ± 1.8	3.7 ± 1.0	51 ± 14
Mertz Depression	−5.9 ± 1.4	2.5 ± 0.9	35 ± 13

Note. A negative flux indicates sea surface CO_2 uptake. A positive NCP indicates net autotrophy.

32.8 and 34.7 (Figure 5a), similar to values reported in previous studies of the Mertz Polynya (Shadwick et al., 2014, 2017). At lower surface salinities ($S < 34.3$), TA and TCO_2 were relatively reduced from subsurface values ($S > 34.3$). The more conservative relationship between TA and salinity in the upper water column indicates that seasonal changes in surface TA were predominantly driven by changes in sea ice dynamics (e.g., sea ice melt), whereas the changes in surface TCO_2 were influenced by additional processes (e.g., photosynthesis and air-sea CO_2 exchange; Figure 5c). Lower sea surface salinities found near the calving face of the MGT in both voyages correspond to TCO_2 minima of ~2,100 μmol kg^{-1} during
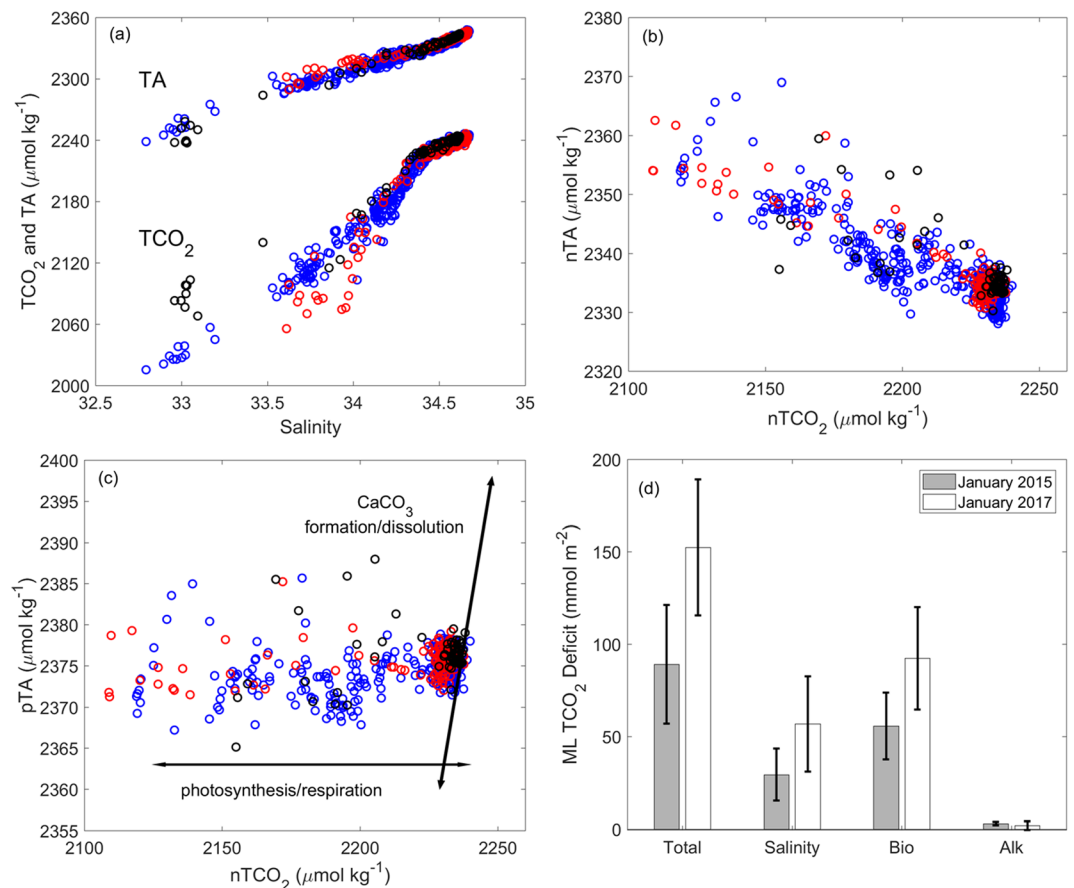
Figure 5. Relationships between (a) salinity and TCO_2 (μmol kg^{-1}) and salinity and TA (μmol kg^{-1}); (b salinity-normalized TA (nTA; μmol kg^{-1}) and salinity-normalized TCO_2 (nTCO_2; μmol kg^{-1}); and (c) salinity-normalized potential alkalinity (pTA; μmol kg^{-1}) and nTCO_2 (μmol kg^{-1}). Color scheme follows Figure 1. (d) Drivers of mixed-layer (ML) TCO_2 (mmol m^{-2}) in January 2015 (gray) and January 2017. Bars represent the total average deficit in TCO_2 and the average contributions due to changes in salinity, biological processes and gas exchange (Bio), and carbonate mineral processes (Alk). Error bars denote one standard deviation.
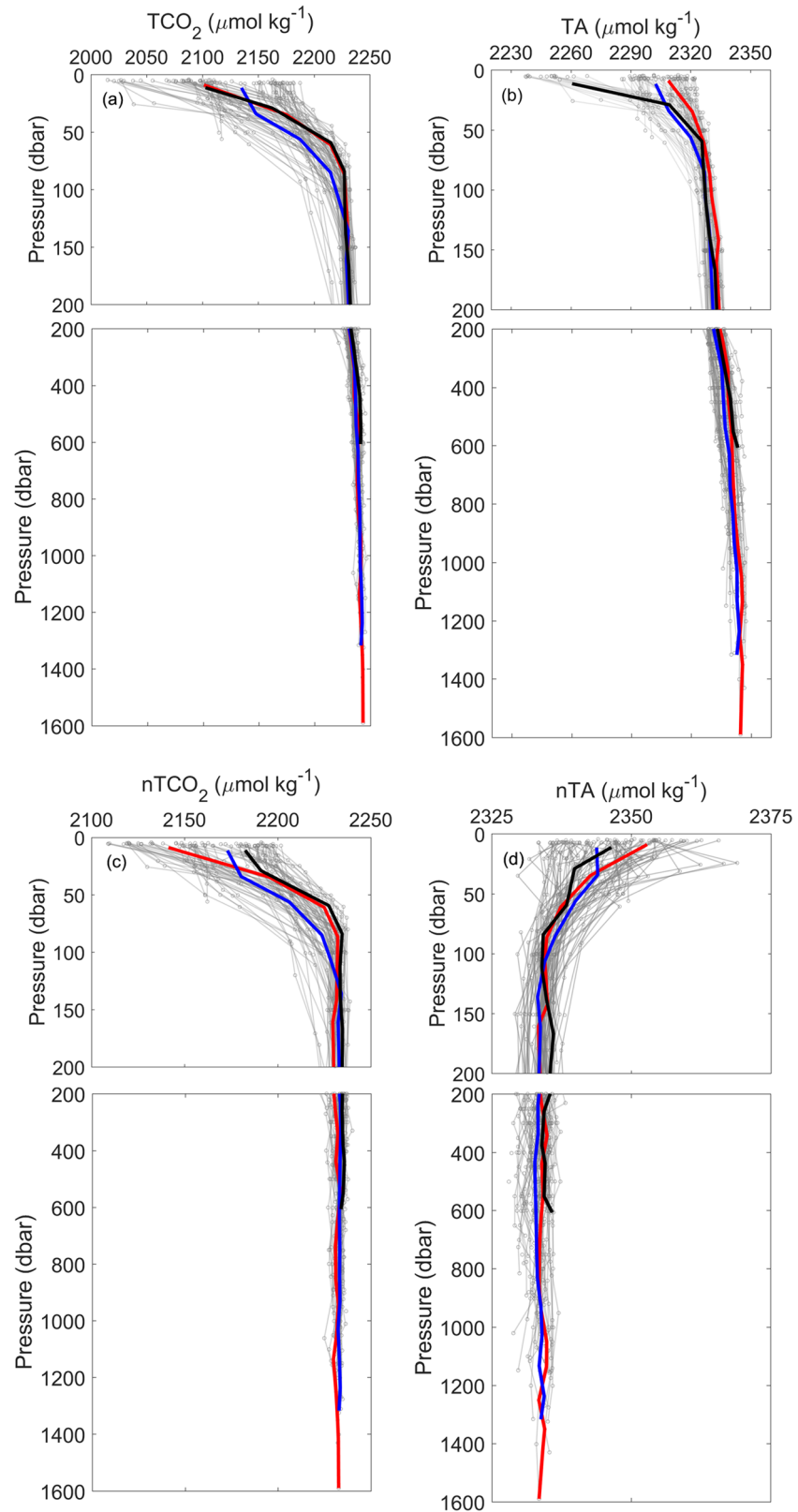
Figure 6. Vertical profiles (gray) of (a) TCO_2 (μmol kg^{-1}), (b) TA (μmol kg^{-1}), (c) $nTCO_2$ (μmol kg^{-1}), and (d) nTA (μmol kg^{-1}), with corresponding average profiles in the Mertz Polynya (blue), Ninnis Polynya (red), and Mertz Depression (black). Color scheme follows Figure 1.

January 2015 and ~2,015 μmol kg^{-1} during January 2017 and TA minima of ~2,290 μmol kg^{-1} during January 2015 and ~2,240 μmol kg^{-1} during January 2017. Average mixed-layer concentrations of TCO$_2$ and TA were overall lower in 2017 (2,079 $\pm$ 36 μmol kg^{-1}; 2,279 $\pm$ 29 μmol kg^{-1}) as compared to 2015 (2,149 $\pm$ 30 μmol kg^{-1}; 2,308 $\pm$ 11 μmol kg^{-1}) but are within range of those previously reported in the Mertz Polynya from 2011 (2,107 $\pm$ 20 μmol kg^{-1}; 2,280 $\pm$ 18 μmol kg^{-1}), 2012 (2,109 $\pm$ 20 μmol kg^{-1}; 2,313 $\pm$ 15 μmol kg^{-1}), and 2013 (2,159 $\pm$ 25 μmol kg^{-1}; 2,315 $\pm$ 10 μmol kg^{-1}; Shadwick et al., 2017).

TCO$_2$ and TA concentrations were normalized to a salinity of 34.5, the average salinity of both data sets (Figure 5b). Salinity normalizing TCO$_2$ and TA accounts for the seasonal variations in salinity due to freshwater input and removal (e.g., sea ice formation and melt), as well as horizontal and vertical mixing, allowing for biogeochemical processes to be distinguished from salinity effects. The negative slope of the linear relationship between salinity-normalized TCO$_2$ (nTCO$_2$) and salinity-normalized TA (nTA) indicates the combined influence of air-sea CO$_2$ exchange, biological processes, and calcium carbonate processes. The exchange of CO$_2$ only impacts concentrations of TCO$_2$ (ingassing of atmospheric CO$_2$ increases TCO$_2$ concentrations) and exerts no influence on TA concentrations. The production of organic matter influences both TCO$_2$ and TA concentrations. Biological production and the fixation of CO$_2$ decreases TCO$_2$ concentrations and marginally increases in TA concentrations due to the assimilation of nitrate by phototrophs (Brewer & Goldman, 1976). As organic matter is remineralized, values of nTCO$_2$ increase and nTA decrease. The impact of biological processes on TA can be accounted for by computing the potential alkalinity (pTA) from nTA and salinity-normalized nitrate (pTA $= \dfrac{\text{TA} + 1.36 \times \text{NO}_3^-}{S} \times 34.5$; Wolf-Gladrow et al., 2007), flattening the pTA-nTCO$_2$ relationship (Figure 5c). An increase in pTA relative to nTCO$_2$ at depth indicates calcium carbonate dissolution in deeper, older water masses on the Adélie Land coast, such as in mCDW (Shadwick et al., 2014). Carbonate dissolution increases pTA and nTCO$_2$ in a ratio of 2:1.

Sea ice formation and melt have been associated with the precipitation and/or dissolution of the calcium carbonate mineral ikaite in Antarctic sea ice (e.g., Dieckmann et al., 2008) influencing the CO$_2$-system chemistry of the underlying surface water (e.g., Jones et al., 2017; Legge et al., 2017). Ikaite precipitation in brine reduces the concentrations of TA and TCO$_2$ in a ratio of 2 to 1, leading to the preferential retention of TA in sea ice and rejection of TCO$_2$ from the sea ice. The net impact of remaining ikaite mineral dissolution in melting sea ice in the spring and summer is an enrichment of TA relative to TCO$_2$ in the surface waters. The conservative relationships between TA and salinity (Figure 5a) and between pTA and nTCO$_2$ (Figure 5c) suggest that the formation and dissolution of calcium carbonate mineral did not influence summertime mixed-layer TCO$_2$ concentrations during these studies, as distinct from the trend for calcium carbonate dissolution in deep mCDW.

The vertical distribution of CO$_2$-system parameters highlights the magnitude of surface variability relative to depth (Figure 6). The vertical profiles of TCO$_2$ and TA indicate a depletion in the surface waters and a convergence below approximately 150 m, in mCDW and DSW. TCO$_2$ concentrations from both data sets converged at a depth of approximately 150 m to values ranging between 2,225 and 2,245 μmol kg^{-1} (mean TCO$_2$ concentration below 150 m = 2,236 $\pm$ 5 μmol kg^{-1}). In the deepest waters within the Ninnis Polynya (depth > 1,300 m), TCO$_2$ concentrations reached a maximum value of 2,244 μmol kg^{-1}.

While the seasonal deficit in mixed-layer TCO$_2$ from the shelf region on the Adélie Land coast was in general greater in 2017 compared to 2015, the magnitudes from both years were within the range of seasonal TCO$_2$ deficits reported from three post calving summers (2011–2013; Figure 5d; Shadwick et al., 2017). In January 2017, mixed-layer TCO$_2$ deficits along the front of the MGT calving face were roughly 60 mmol C m^{-2} greater than in 2015. While in both years the majority of this deficit was attributed to biological production, on average, a slightly larger proportion of the TCO$_2$ deficit was attributed to an increased dilution from sea ice melt in 2017 (approximately 38%) than in 2015 (approximately 33%; Figure 5d). The larger volumes of sea ice melt water during summer 2017 produced a shallower and more stable mixed layer (13 $\pm$ 1 m) as compared to summer 2015 (23 $\pm$ 9 m), consistent with a widespread lower sea surface salinity in 2017 (Figure 3b). These more recent observations continue to support the case of an enhancement in biological productivity relative to precalving polynya configuration due to more favorable conditions for phytoplankton growth (i.e., shallower mixed layers and greater light availability), particularly in proximity to the MGT,

that outweighs the opposing dilution effect from melting sea ice years after the glacial tongue calving (Moreau et al., 2019; Shadwick et al., 2017).

4.4. NCP

NCP was estimated on both voyages as the depth-integrated (surface to 100 m) difference between observed summer $nTCO_2$ and inferred winter $nTCO_2$ concentrations (Figures 3g, 3h, and 6c). Wintertime $nTCO_2$ was estimated from concentrations at 150 m depth, where values begin to converge with depth in deeper water masses ($nTCO_2^{winter}$ = 2,233 ± 3 μmol kg^{-1}, n = 35). Unlike the subsurface waters, mixed-layer TCO_2 concentrations in the Mertz and Ninnis Polynyas were highly variable both regionally and between years, although some broad trends emerge (Table 2). The largest 100 m biological TCO_2 deficits were found in the open surface waters adjacent to the MGT during both voyages. Along the calving edge of the MGT, 100 m TCO_2 deficits were consistent between in the two sampling years: 4.3 to 5.6 mol C m^{-2} (mean = 5.1 mol C m^{-2}) in 2017 and 3.2 to 5.3 mol C m^{-2} in 2015 (mean = 4.4 mol C m^{-2}), corresponding to NCP rates of 60 to 78 mmol C m^{-2} day^{-1} and NCP of 42 to 72 mmol C m^{-2} day^{-1}, respectively. This pattern of the largest TCO_2 deficits near the MGT relative to the greater Adélie Land shelf region within a sampling year was consistently seen in previous years (Shadwick et al., 2017) and agrees well with observed spatial patterns of depth-integrated phytoplankton biomass and chlorophyll a concentration and with $\Delta O_2/Ar$ estimates (Moreau et al., 2019). The ranges of TCO_2 deficits and NCP decrease offshore along the previous western edge of the MGT, with values between 1.9 and 3.4 mol C m^{-2} and 26 to 48 mmol C m^{-2} day^{-1}, respectively. The ranges in NCP are in good agreement with previous studies, and these rates are considerably greater than NCP rates in the precalving conditions likely due in part to an increase in dissolved iron delivery from sea ice melt water and/or stronger summer stratification improving light conditions since the MGT calving (Shadwick et al., 2017). TCO_2 deficits and NCP in the Ninnis Polynya were similar, ranging between 3.6 and 4.7 mol C m^{-2} and 50 and 65 mmol C m^{-2} day^{-1}, respectively, with the exception of a few stations toward the coast. In waters overlying the Adélie Depression and Mertz Depression, 100 m TCO_2 deficits were smaller, ranging between 1.5 and 4.1 mol C m^{-2}, corresponding to smaller NCP rates of 20 to 55 mmol C m^{-2} day^{-1}.

4.5. Inorganic Carbon Transport With DSW

There are regional and seasonal patterns in Transport^{DSW} and CO_2^{DSW} across the polynya model boundaries (Figure 7; Table 3). DSW is exported off the shelf break along Adélie Land coast from three regions: the northern regions across the Adélie Sill and Adélie Bank (Mertz Polynya) and the Mertz Sill and Mertz Bank (Ninnis Polynya) and from the western side of the Mertz Polynya. The greatest DSW outflow from the Adélie Land coast occurred through the Adélie Sill from the northern Mertz Polynya with an annual mean export of 222 ± 105 mSv, peaking during the austral winter months (Figure 7c). DSW export through the northern Mertz region begins to increase in May when sea ice production erodes summer stratification, followed by a peak in October due to a maximum in water column convection and a slow decline through January into the austral summer. Correspondingly, the maximum CO_2^{DSW} (183 ± 100 Tg C yr^{-1}) was exported from the northern region of the Mertz Polynya, with seasonal variation a function of seasonality in volume transport as well as the concentration of TCO_2 in the transported volume. Although the denser DSW fractions are richer in inorganic carbon, the smaller transport of those denser fractions delivered less carbon to the deep ocean than the lighter DSW fractions with lower concentrations of TCO_2 and larger volume transport.

The northern Ninnis Polynya has a weaker seasonal cycle, and the lightest fraction of DSW is exported through the Mertz Sill (Figure 7d). The model-derived transport estimates in the postcalving MGT scenario indicated that no waters denser than 27.92 kg m^{-3} were exported from the region, and a net annual mean of 178 ± 74 mSv of lighter DSW fractions was exported. Because of the weaker seasonal transport cycle, there is a smaller seasonal variability in CO_2^{DSW} from the northern Ninnis. On average, there was an export of 145 ± 75 Tg C yr^{-1} from the northern Ninnis Polynya.

The densest source of DSW (σ_θ > 28.20 kg m^{-3}) is exported from the western edge of the Mertz Polynya, west of the Adélie Depression and Adélie Sill, with an annual mean outflow of 141 ± 54 mSv and a CO_2^{DSW} outflow of 117 ± 52 Tg C yr^{-1} (Figure 7a). Kusahara et al. (2017) identify this DSW source as originating from
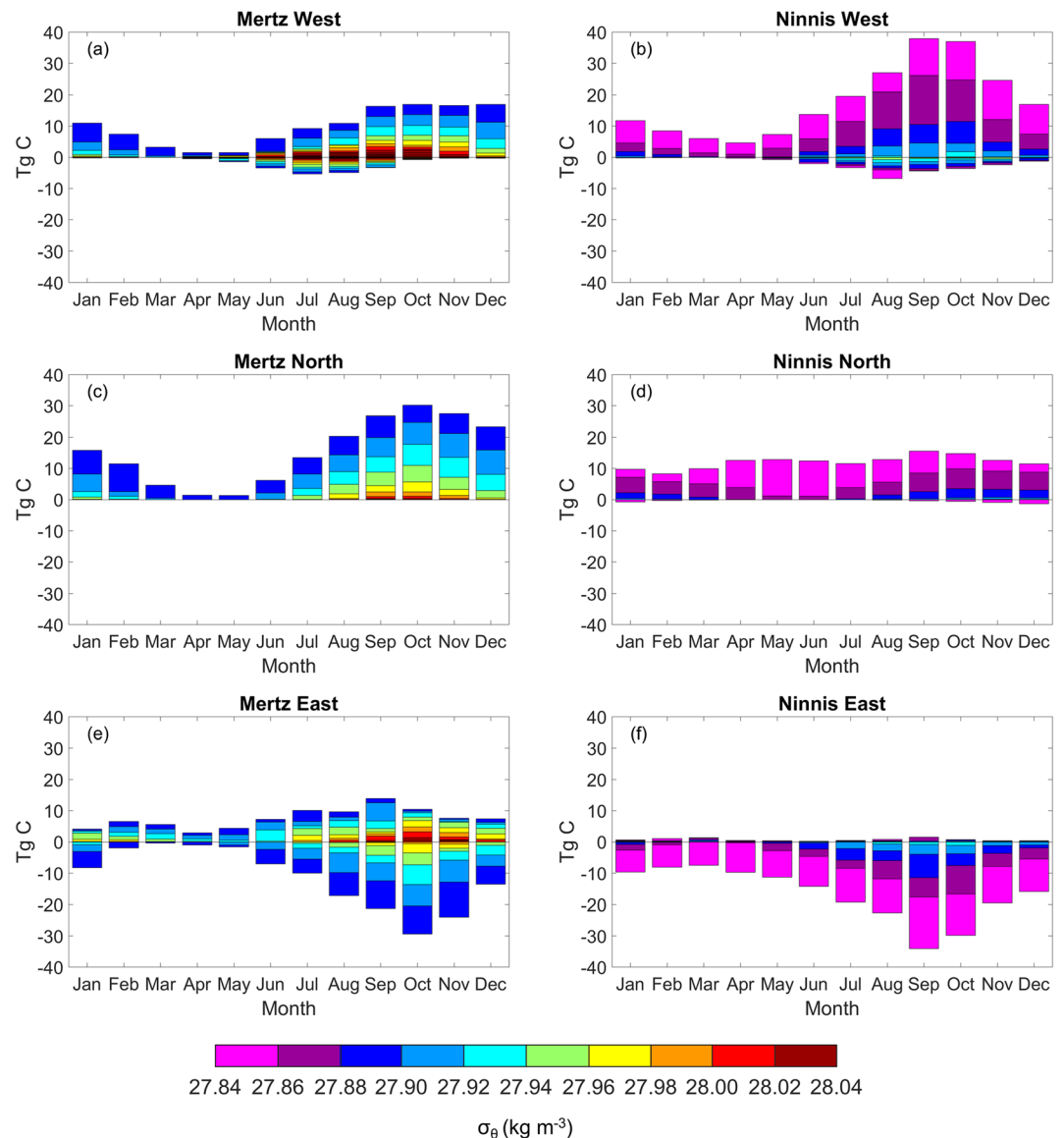
Figure 7. Monthly averaged inorganic carbon transport (Tg C month^{-1}) with DSW from the (a, b) western, (c, d) northern, and (e, f) eastern boundaries of the Mertz Polynya (left column) and Ninnis Polynyas (right column) as binned by potential density anomaly in 0.02 kg m^{-3} increments (color axis). Monthly DSW volume transports obtained from C2000 (2001–2013) case (Kusahara et al., 2017). Denser DSW fractions are indicated in deep red. Positive values indicate outflows.

the overflows of DSW production in the Adélie Depression which are then ultimately transported off the shelf break farther west through the bathymetric sill found near the D'Urville Trough Sill between 136°E and 140°E, with peak export occurring at a 2-month time lag (in November) relative to waters leaving through the Adélie Sill.

These three DSW export pathways, the northern boundaries of the Mertz and Ninnis Polynyas and the western boundary of the Mertz Polynya, deliver a net of 420 ± 210 Tg C yr^{-1} in DSW off the continental shelf along the Adélie Land coast. This DSW outflow is partially compensated by a DSW inflow pathway at the eastern side of the Ninnis Polynya that delivers a net of 193 ± 161 Tg C yr^{-1} into the region. A portion of this inflow from the eastern Ninnis Polynya flows into the eastern Mertz Polynya. Accounting for both inflow

Table 3

Annual DSW Volume Transport (mSv) and Inorganic C Transport (Tg C yr^{-1}) With DSW From the Mertz Polynya (DSW: $\sigma_\theta \geq 27.88$ kg m^{-3}) and Ninnis Polynya (DSW: $\sigma_\theta \geq 27.84$ kg m^{-3}) Averaged Between 2011 and 2013

Region		Volume transport (mSv)		Inorganic C transport (Tg C yr^{-1})	
		Inflow	Outflow	Inflow	Outflow
West					
	Mertz	23 ± 12	141 ± 54	20 ± 11	117 ± 52
	Ninnis	29 ± 6	261 ± 170	25 ± 6	214 ± 153
North					
	Mertz	—	222 ± 105	—	183 ± 100
	Ninnis	6 ± 5	178 ± 74	4 ± 5	145 ± 75
East					
	Mertz	166 ± 132	107 ± 30	135 ± 118	90 ± 30
	Ninnis	245 ± 186	10 ± 7	201 ± 164	8 ± 6

and outflow DSW pathways on the Adélie Coast, approximately 227 ± 115 Tg C yr^{-1} is exported from the continental shelf to deep water offshore.

5. Discussion

5.1. Biogeochemical Variability in the Surface Mixed Layer

The Mertz Polynya system has been well studied relative to others in the East Antarctic (Rintoul, 1998; Shadwick et al., 2017; Williams et al., 2010; Williams & Bindoff, 2003). CO_2-system observations over the last decade have indicated a large interannual variability in summer surface waters, influenced predominantly by seasonal and regional sea ice dynamics and biological processes that impose correspondingly large variations in mixed-layer TCO_2 concentrations. Prior to 2017, heavy sea ice conditions to the west of the Ninnis Glacier made the area inaccessible by ship. Grounded icebergs and fast ice provided a barrier to the westward advection of pack ice. These features were persistent over several decades (e.g., Frezzotti et al., 1998; Massom, 2003) but were disrupted due to the regime shift in sea ice production and polynya activity after the 2010 MGT calving (Ohshima et al., 2016; Tamura et al., 2012). New observations from within the Ninnis Polynya east of the Mertz Polynya reveal similarities in CO_2-system properties between the two regions. The Ninnis Polynya experienced high rates of NCP and was a sink of CO_2 from the atmosphere with a strong undersaturation in fCO$_2$ during the austral summer. However, the air-to-sea CO_2 fluxes were relatively small in the Ninnis Polynya compared to Mertz Polynya due to weak summer winds during observations.

5.2. Sources of Inorganic Carbon to DSW

The outflow of DSW carries approximately 227 ± 115 Tg C yr^{-1} from the Mertz and Ninnis Polynyas (Figures 7 and 8b). The seasonal cycle of DSW formation and export is primarily driven by the growth and decay of sea ice at the surface and by the seasonally variable, lateral input of warm, salty mCDW at mid-depths across the shelf break (Williams et al., 2008). Intrusions of mCDW erode the summer mixed layer and precondition the water column during the spring-autumn transition (Williams et al., 2011). The
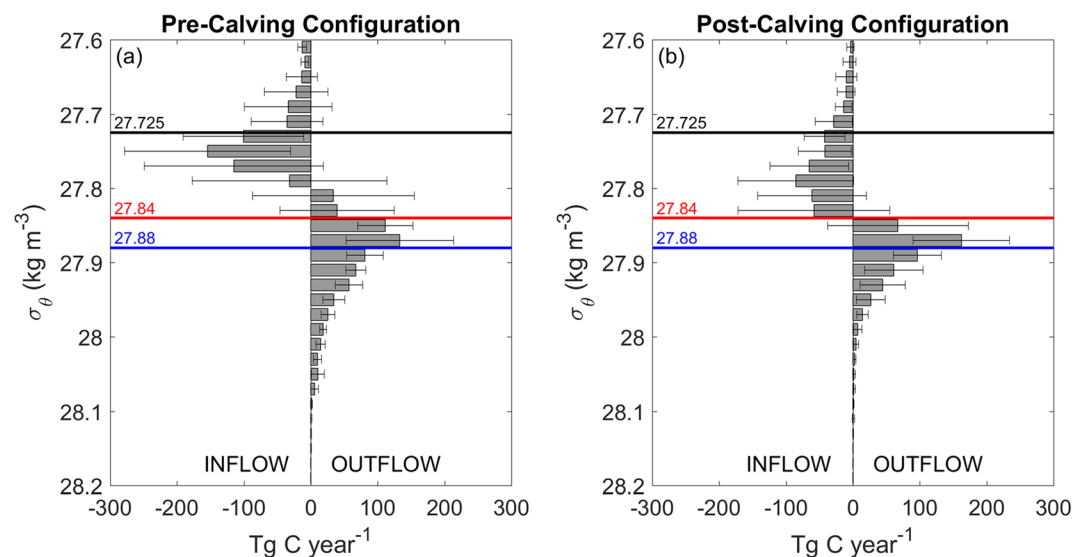
Figure 8. Subsurface fluxes of inorganic carbon (Tg C yr^{-1}) with potential density anomaly (σ_θ; kg m^{-3}) from the Adélie Land coast in the (a) precalving and (b) postcalving configuration of the Mertz Polynya. Black, red, and blue lines delineate the upper boundaries of mCDW ($\sigma_\theta > 27.725$ kg m^{-3}) and DSW ($\sigma_\theta > 27.84$ kg m^{-3} in the Ninnis Polynya and $\sigma_\theta > 27.88$ kg m^{-3} in the Mertz Polynya).

predominant properties of mCDW are derived from the offshore, relatively uniform water mass Upper Circumpolar Deep Water (UCDW) from the ACC (Whitworth et al., 1998). As UCDW shoals toward the Antarctic continental shelf, it mixes with overlying low-salinity AASW and/or cold, low-salinity shelf waters south of the Antarctic Slope Front to produce mCDW (Rintoul, 1998). As mCDW moves from the slope to the shelf, it becomes cooler, fresher, more depleted in TCO_2 (relative to its offshore source), and likely enriched with particulate organic matter by mixing with the remnant summer AASW. The source mCDW used in this budget analysis is relatively highly modified ($\theta < -1°C$, $S \approx 34.5$) and depleted in TCO_2, ($2{,}234 \pm 4$ $\mu mol\ kg^{-1}$) compared to mCDW near the slope ($\theta > 0°C$, $S \approx 34.6$) where TCO_2 concentrations were found to be higher in summer 2007/2008 ($2{,}250$ $\mu mol\ kg^{-1}$; Shadwick et al., 2014). The biogeochemical characteristics of shelf water are modified by primary productivity and the associated TCO_2 reduction in the summer surface mixed layer. This signal is transferred to DSW by deep convection in winter (Shadwick et al., 2014). As a result, DSW outflows are also likely enriched in organic matter, as observed in the dense overflows from the Ross Sea (Bercovici et al., 2017) and Cape Darnely and Prydz Bay in East Antarctica (Fang et al., 2018; Murakami et al., 2020).

Because the incoming mCDW is not dense enough to sink off the continental shelf, an additional source of salinity to the winter mixed layer from local shelf waters is required for the formation of DSW. This additional contribution of salinity is supplied by brine rejection during sea ice formation. In Adélie Land, the persistent coastal Mertz and Ninnis polynyas have among the highest rates of sea ice production in the coastal Antarctic (Tamura et al., 2016), with enhanced sea ice production facilitated by the presence of a glacial tongue barrier. While the locally high rates of sea ice production are critical to the formation of DSW, the preconditioning of the water column with high TCO_2 sourced from mCDW is responsible for the bulk of the biogeochemical TCO_2 signal in DSW on the Adélie Coast (Figure 8). The observed increase of TCO_2 in DSW ($2{,}241 \pm 2$ $\mu mol\ kg^{-1}$) relative to TCO_2 in mCDW ($2{,}234 \pm 4$ $\mu mol\ kg^{-1}$) as observed in summer can be accounted for by the difference in salinity (S in DSW: 34.62 ± 0.03; S in mCDW: 34.52 ± 0.04) and thus is attributed to the addition of TCO_2 with brine to DSW during sea ice formation from the previous winter season. When both the inflow of inorganic carbon with mCDW and the outflow of inorganic carbon with DSW are considered, there is approximately 137 ± 68 Tg C yr^{-1} delivered from the continental shelf of Adélie Land to offshore in the lower levels ($\sigma_\theta \geq 27.725$ kg m^{-3}; mCDW to depth) of the water column (Figure 8b). The enrichment of TCO_2 in DSW due to brine rejection (inferred from the change in salinity) and the greater volumetric flow rate of DSW relative to mCDW result in the net export of inorganic carbon with DSW.

The carbon cycle in the Southern Ocean has been traditionally described by vertical overturning circulation that delivers cold, dense AABW into the ocean interior. Water mass transformations between shelf water near the Antarctic continent and mid-depth, warmer water from the ACC influence the biogeochemical and physical properties of AABW. Recent work by MacGilchrist et al. (2019) describes the expansion of this two-dimensional, overturning framework of the carbon cycle to a three-dimensional framework that includes the horizontal circulation of mid-depth waters in the subpolar Southern Ocean. In their analysis of carbon transport from the Weddell Gyre, the authors highlight the role of biological production in the mixed layer and subsequent organic matter remineralization in the mid-depth Circumpolar Deep Water (CDW) in the central gyre, such that outflowing CDW is enriched in TCO_2 relative to its inflowing source from the ACC as the water circulates clockwise. Over the full-depth water column in the Weddell Gyre, the horizontal circulation transports 72 ± 4 Tg C yr^{-1} out of the region, predominantly attributed to the strong local biological pump (MacGilchrist et al., 2019). This horizontal inorganic carbon export is offset by a full-depth import of 18 ± 10 Tg C yr^{-1} by vertical overturning, leading to a total export of 53 ± 10 Tg C yr^{-1} over the full depth of the Weddell Gyre (MacGilchrist et al., 2019).

Following the analysis by MacGilchrist et al., 2019, we compute the full-depth export from the Adélie Land in the postcalving polynya configuration of 3 ± 2 Tg C yr^{-1} that represents the sum of the overturning and horizontal transports (i.e., total transport) (Figure 8b). This quantity is significantly smaller than the Weddell Sea Gyre total export of 53 ± 10 Tg C yr^{-1} (about 5%; MacGilchrist et al., 2019) and global particulate organic matter export across 2,000 m of 430 Tg C yr^{-1} (less than 1%; Honjo et al., 2008). Compared to the open-ocean subpolar Weddell Sea Gyre, the coastal Mertz and Ninnis Polynyas produce and transport less DSW on a smaller spacial scale over narrow, shallow continental shelf and are influenced by a more

modified form of CDW associated with lower concentration of TCO_2. In the Adélie Land system, the high rate of winter sea ice production (and the rejection of salinity) is the major process enriching TCO_2 in the exported water rather than the local biological pump as in the Weddell Sea Gyre (MacGilchrist et al., 2019).

5.3. Impact of the MGT Calving on Inorganic Carbon Export With DSW

The observed postcalving mean TCO_2 concentration in DSW ($2{,}241 \pm 2\,\mu\text{mol kg}^{-1}$) compares well to the previously reported concentration of $2{,}238\,\mu\text{mol kg}^{-1}$ from the Mertz Polynya during summer 2008 before the MGT calving (Shadwick et al., 2014). We therefore use these postcalving summer data sets to characterize the inorganic carbon export with DSW for the precalving configuration using model-derived transport estimates of the control case (CTRL) averaged from 2001 to 2013 ($n = 13$; Figure 8a; Kusahara et al., 2017). In the precalving configuration in Adélie Land, approximately 327 ± 89 Tg C yr^{-1} was exported with DSW below 27.88 kg m^{-3} and 140 Tg C yr^{-1} was imported with mCDW, leading to a net export of 243 ± 194 Tg C yr^{-1} from the region at depth ($\sigma_\theta \geq 27.725$ kg m^{-3}). This export is larger than the postcalving estimate of $\text{CO}_2{}^{\text{DSW}}$ due to greater DSW volume transport in the precalving configuration of the Mertz Polynya. The MGT calving led to a decrease in winter sea ice production, resulting in a decrease in the density of exported DSW (Kusahara et al., 2011b; Shadwick et al., 2013). In the precalving configuration of the region, we compute a full-depth export of 4 ± 2 Tg C yr^{-1} (Figure 8a), indicating there was a 25% reduction in inorganic carbon export due to the glacial tongue calving (assuming an equal concentration of TCO_2). This highlights the sensitivity of inorganic carbon export from Adélie Land to the strength of the polynyas and the changes in the rate of DSW formation and export.

A previous study by Shadwick et al. (2014) estimated that between 320 and 560 Tg CO_2 (equivalent to approximately 85 to 150 Tg C) is exported annually across the Adélie Sill from the Mertz Polynya with DSW outflow in the precalving configuration. Similar to our analysis, the authors combined the observed summertime concentration of TCO_2 in DSW from the Mertz Polynya with model-derived volumetric DSW transport estimates from the Adélie Land coast obtained from a coupled sea ice-ocean model by Kusahara et al. (2011a). In contrast to our study, the authors bound their estimates by assuming an upper and lower bound for the critical density of DSW export of (27.88 and 27.80 kg m^{-3}, respectively) and use annual average DSW export rates for each critical density threshold (0.21 and 0.37 Sv, respectively). Additionally, mixing between outflowing DSW and the entrainment of offshore (relatively TCO_2-enriched) mCDW was explicitly accounted for. Using our approach, including the seasonal variations in DSW export yields larger estimates of inorganic carbon export from the Adélie Sill in the Mertz Polynya.

5.4. A Continental Shelf Pump for CO_2 in DSW Formation Regions

Adélie Land is one of four main regions of DSW production around the coast of Antarctica. The transport of CO_2 into the bottom water in East Antarctica has been observed by Takahashi and Chipman (2012), who use measurements of TCO_2 and the partial pressure of CO_2 (pCO_2) from 1992 World Ocean Circulation Experiment (WOCE) to track the fate of CO_2 from the coast of Wilkes Land (168–173°E), farther east of the Adélie Land coast. Their analysis suggests a transport of atmospheric CO_2 from the shelf waters into AABW due to the sinking of Wilkes Land shelf water that entrains TCO_2-rich CDW and ultimately mixes with a dense plume of TCO_2-rich deep water originating from the Ross Sea. This process suggests a transport pathway for atmospheric CO_2 into the AABW layer from the continental shelf, as the shelf waters had absorbed atmospheric CO_2 in summer. In contrast to this CSP, similarly outlined by Tsunogai et al. (1999), the dominant fraction of inorganic carbon in DSW formed in Adélie Land is sourced from mCDW, containing much older CO_2, with a minor contribution of inorganic carbon from shelf waters in contact with the atmosphere. This sequestration of older carbon from mCDW to the deeper ocean in AABW nonetheless reduces the possibility for these high CO_2 waters to exchange with the atmosphere if they were to remain on the shelf. While this mechanism at present may make a small impact on sequestering anthropogenic atmospheric CO_2 to the abyssal ocean, this process could be more significant in the future under conditions of continued ocean uptake of anthropogenic CO_2 and accumulation in the midwater column.

In contrast to systems that form bottom water, coastal Antarctic regions that do not supply water to the deep ocean (e.g., the Amundsen Sea Polynya) lack the circulation to transport carbon into the ocean interior, such that organic and inorganic carbon may not be sequestered effectively (e.g., Lee et al., 2017). Deep winter mixing on the continental shelf in the Mertz and Ninnis Polynyas enhances the exchange between shallow shelf

and deeper waters, facilitating the transport of carbon to the ocean interior. In this region of deep water formation, the lateral movement of DSW from the Adélie and Mertz Depressions into the deep ocean during DSW export and AABW formation creates a CSP pathway for the delivery of predominantly midlayer-derived carbon to the deep ocean.

6. Conclusion

Results from new observations in the Mertz Polynya and Ninnis Polynya in Adélie Land show the open surface waters continue to support high levels of biological productivity and sustain a sink for atmospheric CO_2 in the summertime. The accumulation of DSW in the bathymetric depressions adjacent to the Mertz and Ninnis Polynyas allows for the properties of waters predominantly formed in winter to be observed in the summertime. Summer observations of TCO_2 in DSW were combined with modeled DSW transport estimates to show that inorganic carbon is transported off the continental shelf into the deep ocean. In contrast to surface mixed-layer concentrations, the concentration of TCO_2 in DSW was found to be similar in both summers, suggesting that the local contribution from summer processes including seasonal NCP and the associated sea surface uptake of atmospheric CO_2 makes a small imprint on the inorganic carbon signature in DSW. The enrichment of TCO_2 in DSW can be accounted for by changes in salinity, suggesting that brine rejection during winter sea ice formation is the main driver, after the winter water column is preconditioned with inflowing, TCO_2-rich mCDW. Based on the limited numer of observations, we assume that the variability in inorganic carbon export from the region is more strongly associated with the variability in the DSW transport rather than with the variability in DSW TCO_2 concentration. We find a 25% reduction in full-depth inorganic carbon export in the postcalving configuration of the Adélie Land coast due to reduced DSW export, highlighting the role of polynya activity on inorganic carbon transport to the deep ocean.

Data Availability Statement

The water column CO_2 system measurements are publically available through the Australian Antarctic Data Centre (at https://data.aad.gov.au/metadata/records/au1402 and https://data.aad.gov.au/metadata/records/AAS_4131_au1602). NCEP Reanalysis data are provided by the NOAA/OAR/ESRL PSD, Boulder, Colorado, USA, from their Web site (at https://www.esrl.noaa.gov/psd/).

References

Aoki, S., Kobayashi, R., Rintoul, S. R., Tamura, T., & Kusahara, K. (2017). Changes in water properties and flow regime on the continental shelf off the Adélie/George V Land coast, East Antarctica, after glacier tongue calving. *Journal of Geophysical Research: Oceans*, *122*, 6277–6294. https://doi.org/10.1002/2017JC012925

Arrigo, K. R., van Dijken, G., & Long, M. (2008). Coastal Southern Ocean: A strong anthropogenic CO_2 sink. *Geophysical Research Letters*, *35*, L21602. https://doi.org/10.1029/2008GL035624

Arrigo, K. R., & van Dijken, G. L. (2003). Phytoplankton dynamics within 37 Antarctic coastal polynya systems. *Journal of Geophysical Research*, *108*(C8), 3271. https://doi.org/10.1029/2002JC001739

Arroyo, M. C., Shadwick, E. H., & Tilbrook, B. (2019). Summer carbonate chemistry in the Dalton Polynya, East Antarctica. *Journal of Geophysical Research: Oceans*, *124*, 5634–5653. https://doi.org/10.1029/2018JC014882

Bates, N. R. (2006). Air-sea CO_2 fluxes and the continental shelf pump of carbon in the Chukchi Sea adjacent to the Arctic Ocean. *Journal of Geophysical Research*, *111*, C10013. https://doi.org/10.1029/2005JC003083

Bercovici, S. K., Huber, B. A., DeJong, H. B., Dunbar, R. B., & Hansell, D. A. (2017). Dissolved organic carbon in the Ross Sea: Deep enrichment and export. *Limnology and Oceanography*, *62*(6), 2593–2603. https://doi.org/10.1002/lno.10592

Bindoff, N. L., Williams, G. D., & Allison, I. (2001). Sea-ice growth and water-mass modification in the Mertz Glacier polynya, East Antarctica, during winter. *Annals of Glaciology*, *33*, 399–406. https://doi.org/10.3189/172756401781818185

Bozec, Y., Thomas, H., Elkalay, K., & de Baar, H. J. W. (2005). The continental shelf pump for CO_2 in the North Sea—Evidence from summer observation. *Marine Chemistry*, *93*(2–4), 131–147. https://doi.org/10.1016/j.marchem.2004.07.006

Brewer, P. G., & Goldman, J. C. (1976). Alkalinity changes generated by phytoplankton growth. *Limnology and Oceanography*, *21*(1), 108–117. https://doi.org/10.4319/lo.1976.21.1.0108

Carmack, E. C., & Foster, T. D. (1975). On the flow of water out of the Weddell Sea. *Deep Sea Research and Oceanographic Abstracts*, *22*(11), 711–724. https://doi.org/10.1016/0011-7471(75)90077-7

Cougnon, E. A., Galton-Fenzi, B. K., Meijers, A. J. S., & Legrésy, B. (2013). Modeling interannual dense shelf water export in the region of the Mertz Glacier Tongue (1992–2007). *Journal of Geophysical Research: Oceans*, *118*, 5858–5872. https://doi.org/10.1002/2013JC008790

Cougnon, E. A., Galton-Fenzi, B. K., Rintoul, S. R., Legrésy, B., Williams, G. D., Fraser, A. D., & Hunter, J. R. (2017). Regional changes in icescape impact shelf circulation and basal melting. *Geophysical Research Letters*, *44*, 11,519–11,527. https://doi.org/10.1002/2017GL074943

Dickson, A. G., Afghan, J. D., & Anderson, G. C. (2003). Reference materials for oceanic CO_2 analysis: A method for the certification of total alkalinity. *Marine Chemistry*, *80*(2–3), 185–197. https://doi.org/10.1016/S0304-4203(02)00133-0

Dickson, A.G., Sabine, C.L., & Christian, J.R. (Eds.) (2007). *Guide to best practices for ocean CO_2 measurements*. PICES Special Publication 3. (p. 191) North Pacific Marine Science Organization, Sydney, B.C., Canada.

Dieckmann, G. S., Nehrke, G., Papadimitriou, S., Göttlicher, J., Steininger, R., Kennedy, H., et al. (2008). Calcium carbonate as ikaite crystals in Antarctic sea ice. *Geophysical Research Letters*, *35*, L08501. https://doi.org/10.1029/2008GL033540

Fang, Z., Yang, W., Chen, M., Stubbins, A., Ma, H., Jia, R., et al. (2018). Transport of dissolved black carbon from the Prydz Bay shelf, Antarctica to the deep Southern Ocean. *Limnology and Oceanography*, *63*(5), 2179–2190. https://doi.org/10.1002/lno.10932

Frezzotti, M., Cimbelli, A., & Ferrigno, J. G. (1998). Ice-front change and iceberg behaviour along Oates and George V coasts, Antarctica, 1912–96. *Annals of Glaciology*, *27*, 643–650. https://doi.org/10.3189/1998AoG27-1-643-650

GEBCO Bathymetric Compilation Group (2019). *The GEBCO_2019 Grid - a continuous terrain model of the global oceans and land*. British Oceanographic Data Centre, National Oceanography Centre, NERC, UK. Retrieved from https://sextant.ifremer.fr/record/01040a3e-e75b-48d1-9ece-e96b4ccdebc3/

Gordon, A. L., & Tchernia, P. (1972). Waters of the continental margin off Adélie coast, Antarctica. In D. E. Hayes (Ed.), *Antarctic oceanology 2: The Australian-New Zealand sector* (Vol. 19, pp. 59–69). New York: American Geophysical Union. https://doi.org/10.1029/AR019p0059

Ho, D. T., Law, C. S., Smith, M. J., Schlosser, P., Harvey, M., & Hill, P. (2006). Measurements of air-sea gas exchange at high wind speeds in the Southern Ocean: Implications for global parameterizations. *Geophysical Research Letters*, *33*, L16611. https://doi.org/10.1029/2006GL026817

Honjo, S., Manganini, S. J., Krishfield, R. A., & Francois, R. (2008). Particulate organic carbon fluxes to the ocean interior and factors controlling the biological pump: A synthesis of global sediment trap programs since 1983. *Progress in Oceanography*, *76*(3), 217–285. https://doi.org/10.1016/j.pocean.2007.11.003

IOC, IHO, & BODC (2003). GEBCO digital atlas. Centenary ed., Intergovernmental Oceanographic Commission, International Hydrographic Organization and British Oceanographic Data Centre, CD-ROM. http://www.gebco.net/data_and_products/gebco_digital_atlas/.

Jacobs, S. S., Amos, A. F., & Bruchhausen, P. M. (1970). Ross Sea oceanography and Antarctic Bottom Water formation. *Deep Sea Research and Oceanographic Abstracts*, *17*(6), 935–962. https://doi.org/10.1016/0011-7471(70)90046-X

Johnson, K. M., Wills, K. D., Butler, D. B., Johnson, W. K., & Wong, C. S. (1993). Coulometric total carbon dioxide analysis for marine studies: Maximizing the performance of an automated gas extraction system and coulometric detector. *Marine Chemistry*, *44*(2–4), 167–187. https://doi.org/10.1016/0304-4203(93)90201-X

Jones, E., Bakker, D., Venables, H., Whitehouse, M., Korb, R., & Watson, A. (2010). Rapid changes in surface water carbonate chemistry during Antarctic sea ice melt. *Tellus B: Chemical and Physical Meteorology*, *62*(5), 621–635. https://doi.org/10.1111/j.1600-0889.2010.00496.x

Jones, E. M., Fenton, M., Meredith, M. P., Clargo, N. M., Ossebaar, S., Ducklow, H. W., et al. (2017). Ocean acidification and calcium carbonate saturation states in the coastal zone of the West Antarctic Peninsula. *Deep-Sea Research Part II: Topical Studies in Oceanography*, *139*, 181–194. https://doi.org/10.1016/j.dsr2.2017.01.007

Kalnay, E., Kanamitsu, M., Kistler, R., Collins, W., Deaven, D., Gandin, L., et al. (1996). The NCEP/NCAR 40-year reanalysis project. *Bulletin of the American Meteorological Society*, *77*(3), 437–471. https://doi.org/10.1175/1520-0477(1996)077<0437:TNYRP>2.0.CO;2

Kusahara, K., Hasumi, H., Fraser, A. D., Aoki, S., Shimada, K., Williams, G. D., et al. (2017). Modeling ocean-cryosphere interactions off Adélie and George V Land, East Antarctica. *Journal of Climate*, *30*(1), 163–188. https://doi.org/10.1175/JCLI-D-15-0808.1

Kusahara, K., Hasumi, H., & Tamura, T. (2010). Modeling sea ice production and dense shelf water formation in coastal polynyas around East Antarctica. *Journal of Geophysical Research*, *115*, C10006. https://doi.org/10.1029/2010JC006133

Kusahara, K., Hasumi, H., & Williams, G. D. (2011a). Dense shelf water formation and brine-driven circulation in the Adélie and George V Land region. *Ocean Modelling*, *37*(3–4), 122–138. https://doi.org/10.1016/j.ocemod.2011.01.008

Kusahara, K., Hasumi, H., & Williams, G. D. (2011b). Impact of the Mertz Glacier Tongue calving on dense water formation and export. *Nature Communications*, *2*(1), 159. https://doi.org/10.1038/ncomms1156

Lacarra, M., Houssais, M.-N., Herbaut, C., Sultan, E., & Beauverger, M. (2014). Dense shelf water production in the Adélie Depression, East Antarctica, 2004–2012: Impact of the Mertz Glacier calving. *Journal of Geophysical Research: Oceans*, *119*, 5203–5220. https://doi.org/10.1002/2013JC009124

Lacarra, M., Houssais, M. N., Sultan, E., Rintoul, S. R., & Herbaut, C. (2011). Summer hydrography on the shelf off Terre Adélie/George V Land based on the ALBION and CEAMARC observations during the IPY. *Polar Science*, *5*(2), 88–103. https://doi.org/10.1016/j.polar.2011.04.008

Lee, S. H., Hwang, J., Ducklow, H. W., Hahm, D., Lee, S. H., Kim, D., et al. (2017). Evidence of minimal carbon sequestration in the productive Amundsen Sea polynya. *Geophysical Research Letters*, *44*, 7892–7899. https://doi.org/10.1002/2017GL074646

Legge, O. J., Bakker, D. C. E., Meredith, M. P., Venables, H. J., Brown, P. J., Jones, E. M., & Johnson, M. T. (2017). The seasonal cycle of carbonate system processes in Ryder Bay, West Antarctic Peninsula. *Deep-Sea Research Part II: Topical Studies in Oceanography*, *139*, 167–180. https://doi.org/10.1016/j.dsr2.2016.11.006

MacGilchrist, G. A., Naveira Garabato, A. C., Brown, P. J., Jullion, L., Bacon, S., Bakker, D. C. E., et al. (2019). Reframing the carbon cycle of the subpolar Southern Ocean. *Science Advances*, *5*(8), eaav6410. https://doi.org/10.1126/sciadv.aav6410

Marinov, I., Gnanadesikan, A., Toggweiler, J. R., & Sarmiento, J. L. (2006). The Southern Ocean biogeochemical divide. *Nature*, *441*(7096), 964–967. https://doi.org/10.1038/nature04883

Marsland, S. J., Bindoff, N. L., Williams, G. D., & Budd, W. F. (2004). Modeling water mass formation in the Mertz Glacier Polynya and Adélie Depression, East Antarctica. *Journal of Geophysical Research*, *109*, C11003. https://doi.org/10.1029/2004JC002441

Marsland, S. J., Church, J. A., Bindoff, N. L., & Williams, G. D. (2007). Antarctic coastal polynya response to climate change. *Journal of Geophysical Research*, *112*, C07009. https://doi.org/10.1029/2005JC003291

Massom, R. A. (2003). Recent iceberg calving events in the Ninnis Glacier region, East Antarctica. *Antarctic Science*, *15*(2), 303–313. https://doi.org/10.1017/S0954102003001299

Massom, R. A., Harris, P. T., Michael, K. J., & Potter, M. J. (1998). The distribution and formative processes of latent-heat polynyas in East Antarctica. *Annals of Glaciology*, *27*(1), 420–426. https://doi.org/10.3189/1998AoG27-1-420-426

McNeil, B. I., Tilbrook, B., & Matear, R. J. (2001). Accumulation and uptake of anthropogenic CO_2 in the Southern Ocean, south of Australia between 1968 and 1996. *Journal of Geophysical Research*, *106*(C12), 31,431–31,445. https://doi.org/10.1029/2000JC000331

Morales Maqueda, M. A., Willmott, A. J., & Biggs, N. R. T. (2004). Polynya dynamics: A review of observations and modeling. *Reviews of Geophysics*, *42*, RG1004. https://doi.org/10.1029/2002RG000116

Moreau, S., Lannuzel, D., Janssens, J., Arroyo, M. C., Corkill, M., Cougnon, E., et al. (2019). Sea ice meltwater and circumpolar deep water drive contrasting productivity in three Antarctic polynyas. *Journal of Geophysical Research: Oceans*, *124*, 2943–2968. https://doi.org/10.1029/2019JC015071

Murakami, K., Nomura, D., Hashida, G., Nakaoka, S. I., Kitade, Y., Hirano, D., et al. (2020). Strong biological carbon uptake and carbonate chemistry associated with dense shelf water outflows in the Cape Darnley polynya, East Antarctica. *Marine Chemistry*, *225*, 103842. https://doi.org/10.1016/j.marchem.2020.103842

Ohshima, K. I., Fukamachi, Y., Williams, G. D., Nihashi, S., Roquet, F., Kitade, Y., et al. (2013). Antarctic Bottom Water production by intense sea-ice formation in the Cape Darnley polynya. *Nature Geoscience*, *6*(3), 235–240. https://doi.org/10.1038/ngeo1738

Ohshima, K. I., Nihashi, S., & Iwamoto, K. (2016). Global view of sea-ice production in polynyas and its linkage to dense/bottom water formation. *Geoscience Letters*, *3*(1), 13. https://doi.org/10.1186/s40562-016-0045-4

Orsi, A. H., Johnson, G. C., & Bullister, J. L. (1999). Circulation, mixing, and production of Antarctic Bottom Water. *Progress in Oceanography*, *43*(1), 55–109. https://doi.org/10.1016/S0079-6611(99)00004-X

Orsi, A. H., Smethie, W. M., & Bullister, J. L. (2002). On the total input of Antarctic waters to the deep ocean: A preliminary estimate from chlorofluorocarbon measurements. *Journal of Geophysical Research*, *107*(C8), 3122. https://doi.org/10.1029/2001JC000976

Pierrot, D., Neill, C., Sullivan, K., Castle, R., Wanninkhof, R., Lüger, H., et al. (2009). Recommendations for autonomous underway pCO$_2$ measuring systems and data-reduction routines. *Deep-Sea Research Part II: Topical Studies in Oceanography*, *56*(8–10), 512–522. https://doi.org/10.1016/j.dsr2.2008.12.005

Rintoul, S. R. (1998). On the origin and influence of Adélie Land bottom water. In *Ocean, ice, and atmosphere: Interactions at the Antarctic continental margin* (Vol. 75, pp. 151–171). New York: American Geophysical Union. https://doi.org/10.1029/ar075p0151

Rosenberg, M. A. (2020). Aurora Australis Marine Science Cruise AU1402 (V2 2014/15), Totten and Mertz Glacier regions - Ship-based CTD data, Ver. 2. *Australian Antarctic Data Centre*. https://doi.org/10.26179/cy3g-kw45

Rosenberg, M. A., & Rintoul, S. R. (2018). Aurora Australis Marine Science Cruise AU1602, Dalton, Mertz and Ninnis CTDs - Oceanographic Field Measurements and Analysis, Ver. 2. *Australian Antarctic Data Centre*. https://doi.org/10.26179/vvdt-fh11

Sarmiento, J. L., Gruber, N., Brzezinski, M. A., & Dunne, J. P. (2004). High-latitude controls of thermocline nutrients and low latitude biological productivity. *Nature*, *427*(6969), 56–60. https://doi.org/10.1038/nature02127

Shadwick, E. H., Rintoul, S. R., Tilbrook, B., Williams, G. D., Young, N., Fraser, A. D., et al. (2013). Glacier tongue calving reduced dense water formation and enhanced carbon uptake. *Geophysical Research Letters*, *40*, 904–909. https://doi.org/10.1002/grl.50178

Shadwick, E. H., Tilbrook, B., & Currie, K. I. (2017). Late-summer biogeochemistry in the Mertz Polynya: East Antarctica. *Journal of Geophysical Research: Oceans*, *122*, 7380–7394. https://doi.org/10.1002/2017JC013015

Shadwick, E. H., Tilbrook, B., & Williams, G. D. (2014). Carbonate chemistry in the Mertz Polynya (East Antarctica): Biological and physical modification of dense water outflows and the export of anthropogenic CO$_2$. *Journal of Geophysical Research: Oceans*, *119*, 1–14. https://doi.org/10.1002/2013JC009286

Sigman, D. M., & Boyle, E. A. (2000). Glacial/interglacial variations in atmospheric carbon dioxide. *Nature*, *407*(6806), 859–869. https://doi.org/10.1038/3503800

Silvano, A., Rintoul, S., & Herraiz-Borreguero, L. (2016). Ocean-ice shelf interaction in East Antarctica. *Oceanography*, *29*(4), 130–143. https://doi.org/10.5670/oceanog.2016.105

Snow, K., Rintoul, S. R., Sloyan, B. M., & Hogg, A. M. C. (2018). Change in dense shelf water and Adélie Land bottom water precipitated by iceberg calving. *Geophysical Research Letters*, *45*, 2380–2387. https://doi.org/10.1002/2017GL076195

Sweeney, C., Gloor, E., Jacobson, A. R., Key, R. M., McKinley, G., Sarmiento, J. L., & Wanninkhof, R. (2007). Constraining global air-sea gas exchange for CO$_2$ with recent bomb ^{14}C measurements. *Global Biogeochemical Cycles*, *21*, GB2015. https://doi.org/10.1029/2006GB002784

Sweeney, C., Hansell, D. A., Carlson, C. A., Codispoti, L. A., Gordon, L. I., Marra, J., et al. (2000). Biogeochemical regimes, net community production and carbon export in the Ross Sea, Antarctica. *Deep Sea Research Part II: Topical Studies in Oceanography*, *47*(15–16), 3369–3394. https://doi.org/10.1016/s0967-0645(00)00072-2

Takahashi, T., & Chipman, D. (2012). CO$_2$ transport in deep waters off Wilkes Land. *Oceanography*, *25*(3), 24–25. https://doi.org/10.5670/oceanog.2012.70

Tamura, T., Ohshima, K. I., Fraser, A. D., & Williams, G. D. (2016). Sea ice production variability in Antarctic coastal polynyas. *Journal of Geophysical Research: Oceans*, *121*, 2967–2979. https://doi.org/10.1002/2015JC011537

Tamura, T., Williams, G. D., Fraser, A. D., & Ohshima, K. I. (2012). Potential regime shift in decreased sea ice production after the Mertz Glacier calving. *Nature Communications*, *3*(1), 826. https://doi.org/10.1038/ncomms1820

Thomas, H., Bozec, Y., Elkalay, K., & de Baar, H. J. W. (2004). Enhanced open ocean storage of CO$_2$ from shelf sea pumping. *Science*, *306*(5701), 1477–1008. https://doi.org/10.1126/science.1103193

Timmermann, R., le Brocq, A., Deen, T., Domack, E., Dutrieux, P., Galton-Fenzi, B., et al. (2010). A consistent data set of Antarctic ice sheet topography, cavity geometry, and global bathymetry. *Earth System Science Data*, *2*(2), 261–273. https://doi.org/10.5194/essd-2-261-2010

Tsunogai, S., Watanabe, S., & Sato, T. (1999). Is there a "continental shelf pump" for the absorption of atmospheric CO$_2$? *Tellus Series B: Chemical and Physical Meteorology*, *51*(3), 701–712. https://doi.org/10.3402/tellusb.v51i3.16468

Wanninkhof, R. (1992). Relationship between wind speed and gas exchange over the ocean. *Journal of Geophysical Research*, *97*(C5), 7373–7382. https://doi.org/10.1029/92JC00188

Wanninkhof, R. (2014). Relationship between wind speed and gas exchange over the ocean revisited. *Limnology and Oceanography: Methods*, *12*(JUN), 351–362. https://doi.org/10.4319/lom.2014.12.351

Weiss, R. F. (1974). Carbon dioxide in water and seawater: The solubility of a non-ideal gas. *Marine Chemistry*, *2*(3), 203–215. https://doi.org/10.1016/0304-4203(74)90015-2

Whitworth, T. III, Orsi, A. H., Kim, S.-J., Nowlin, W. D., & Locarnini, R. A. (1998). Water masses and mixing near the Antarctic slope front. In *Ocean, ice, and atmosphere: Interactions at the Antarctic continental margin* (pp. 1–27). New York: American Geophysical Union. https://doi.org/10.1029/ar075p0001

Williams, G. D., Aoki, S., Jacobs, S. S., Rintoul, S. R., Tamura, T., & Bindoff, N. L. (2010). Antarctic Bottom Water from the Adélie and George v Land coast, East Antarctica (140–149°E). *Journal of Geophysical Research*, *115*, C04027. https://doi.org/10.1029/2009JC005812

Williams, G. D., & Bindoff, N. L. (2003). Wintertime oceanography of the Adélie Depression. *Deep Sea Research Part II: Topical Studies in Oceanography*, *50*(8–9), 1373–1392. https://doi.org/10.1016/S0967-0645(03)00074-2

Williams, G. D., Bindoff, N. L., Marsland, S. J., & Rintoul, S. R. (2008). Formation and export of dense shelf water from the Adélie Depression, East Antarctica. *Journal of Geophysical Research*, *113*, C04039. https://doi.org/10.1029/2007JC004346

Williams, G. D., Hindell, M., Houssais, M. N., Tamura, T., & Field, I. C. (2011). Upper ocean stratification and sea ice growth rates during the summer-fall transition, as revealed by elephant seal foraging in the Adélie Depression, East Antarctica. *Ocean Science*, *7*(2), 185–202. https://doi.org/10.5194/os-7-185-2011

Wolf-Gladrow, D. A., Zeebe, R. E., Klaas, C., Körtzinger, A., & Dickson, A. G. (2007). Total alkalinity: The explicit conservative expression and its application to biogeochemical processes. *Marine Chemistry*, *106*(1–2), 287–300. https://doi.org/10.1016/j.marchem.2007.01.006

Yager, P. L., Wallace, D. W. R., Johnson, K. M., Smith, W. O., Minnett, P. J., & Deming, J. W. (1995). The northeast water polynya as an atmospheric CO_2 sink: A seasonal rectification hypothesis. *Journal of Geophysical Research*, *100*(C3), 4389–4398. https://doi.org/10.1029/94JC01962

Zhao, C. L., & Tans, P. P. (2006). Estimating uncertainty of the WMO mole fraction scale for carbon dioxide in air. *Journal of Geophysical Research*, *111*, D08S09. https://doi.org/10.1029/2005JD006003